

AD-A075 007

ILLINOIS UNIV AT CHICAGO CIRCLE DEPT OF PHYSICS
TOPOGRAPHIC EXAMINATION OF SEMICONDUCTOR SYSTEMS. (U)
JUL 79 R L BROWN, S SUNDARAM, P M RACCAH

F/G 20/12

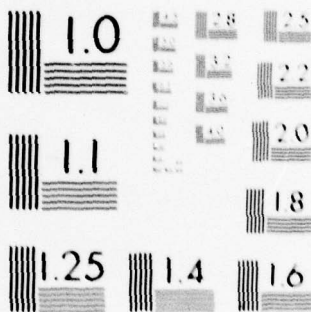
N00173-78-C-0437

UNCLASSIFIED

NL

| OF |
AD
A075007





MICROCOPY RESOLUTION TEST CHART
 NATIONAL BUREAU OF STANDARDS-1963-A

LEVEL II

12

ADA 075007

6
TOPOGRAPHIC EXAMINATION OF SEMICONDUCTOR SYSTEMS.

10
R. L. Brown
S. Sundaram
P. M. Racciah

Department of Physics
University of Illinois at Chicago Circle
Chicago, Illinois 60680

DDC
REGISTERED
OCT 12 1979
E

11
July 1979

12
57

9
ANNUAL TECHNICAL REPORT,
1 June 1978 - 30 June 1979

Prepared for
NAVAL RESEARCH LABORATORY
ELECTRONICS MATERIAL TECHNOLOGY BRANCH
Washington, D.C. 20375

This document has been approved
for public release and sale; its
distribution is unlimited.

DDC FILE COPY

15
NRL Contract No. N00173-78-C-0437

392775

79 10 12 079

13

UNCLASSIFIED

SECURITY CLASSIFICATION OF THIS PAGE (When Data Entered)

REPORT DOCUMENTATION PAGE		READ INSTRUCTIONS BEFORE COMPLETING FORM
1. REPORT NUMBER	2. GOVT ACCESSION NO.	3. RECIPIENT'S CATALOG NUMBER
4. TITLE (and Subtitle) TOPOGRAPHIC EXAMINATION OF SEMICONDUCTOR SYSTEMS		5. TYPE OF REPORT & PERIOD COVERED Annual Technical Report June 1, 1978-June 30, 1979
		6. PERFORMING ORG. REPORT NUMBER
7. AUTHOR(s) R.L. Brown, S. Sundaram, and P.M. Raccah University of IL, Chicago, IL 60680		8. CONTRACT OR GRANT NUMBER(s) N00173-78-C-0437 <i>new</i>
9. PERFORMING ORGANIZATION NAME AND ADDRESS University of Illinois Chicago, Illinois 60680		10. PROGRAM ELEMENT, PROJECT, TASK AREA & WORK UNIT NUMBERS
11. CONTROLLING OFFICE NAME AND ADDRESS Naval Research Laboratory Washington, D.C. 20375		12. REPORT DATE July 1979
		13. NUMBER OF PAGES
14. MONITORING AGENCY NAME & ADDRESS (if different from Controlling Office)		15. SECURITY CLASS. (of this report) Unclassified
		15a. DECLASSIFICATION/DOWNGRADING SCHEDULE
16. DISTRIBUTION STATEMENT (of this Report) Approved for Public release; distribution unlimited.		
17. DISTRIBUTION STATEMENT (of the abstract entered in Block 20, if different from Report)		
18. SUPPLEMENTARY NOTES		
19. KEY WORDS (Continue on reverse side if necessary and identify by block number) Topographic mapping Annealing effects Electroreflectance Gallium Arsenide Carrier concentration Indium phosphide Ion implantation		
20. ABSTRACT (Continue on reverse side if necessary and identify by block number) Using the electrolyte electroreflectance (EER) technique, a systematic characterization of GaAs and InP as well as quaternary alloy InGaAsP has been made. Those materials grown at the Naval Research Laboratory include unimplanted samples and those implanted with Be, Se, and Si ions. Besides topographic examination of uniformity of carrier concentration, the spectra have been analyzed and effects of implantation and anneal procedures on the transition energies have been examined. (see over)		

DD FORM 1 JAN 73 1473

EDITION OF 1 NOV 68 IS OBSOLETE
S/N 0102-LF-014-6601

next page
SECURITY CLASSIFICATION OF THIS PAGE (When Data Entered)

The results of characterization have been provided as "feed back" information for the materials growth program at NRL. EER technique is shown to be an unusually sensitive tool in the characterization of these semiconducting materials.

CONTENTS

ABSTRACT 1

INTRODUCTION 2

EXPERIMENTAL ARRANGEMENT 3

CHARACTERIZATION OF GaAs 7

 A. Unimplanted Samples of GaAs 8

 B. Implanted Samples of GaAs 15

CHARACTERIZATION OF InP 34

 A. Unimplanted Samples of InP 34

 B. Implanted Samples of InP 39

 C. Quaternary Alloy InGaAsP 39

ELECTROREFLECTANCE LINESHAPES 44

ACKNOWLEDGMENT 47

REFERENCES 48

CAPTIONS FOR FIGURES 49

Accession For	
NTIS G&I	<input checked="" type="checkbox"/>
DDC TAB	<input type="checkbox"/>
Unannounced	<input type="checkbox"/>
Justification	
By _____	
Distribution/	
Availability Codes	
Dist	Avail and/or special
A	

ABSTRACT

Using the Electrolyte electroreflectance (EER) technique a systematic characterization of the III-V semiconductor materials of GaAs and InP as well as the quaternary alloy InGaAsP has been made. All these materials (GaAs, InP) were grown at the Naval Research Laboratory and they include unimplanted samples as well as those implanted with Be, Se, and Si ions. The carrier concentration uniformity has been evaluated using EER topographic examination. The spectra have been analyzed and the effects of implantation and post-implantation annealing procedures on the characteristic line shape features have been examined. The results of characterization have provided the information for use in the materials growth program of NRL and device development program of the Navy. The EER technique is shown to be an unusually sensitive tool to characterize the semiconductors and even inversion layers in some cases.

I. INTRODUCTION

The need for proper characterization of materials and processing procedures as an aid in materials growth and device development effort is well established. The program described in this report is part of a large scale and coordinated effort with the Naval Research Laboratory on the thorough characterization of GaAs and InP for use in opto-electronic devices. The over-all objective of the present program is to provide rapid "feed back" information on the characteristics of GaAs and InP grown at NRL and subjected to ion-implantation by the NRL group. This has been achieved using the techniques of modulation spectroscopy,¹ more specifically through the use of the most efficient non-destructive technique of electrolyte electroreflectance^{2,3} (EER). The characteristic electroreflectance spectra of the materials have been studied and the topographic scans of the distribution of surface carrier concentrations have been made for the semiconductors of GaAs and InP. The investigations in this program extended to the above materials implanted with Be, Se, and Si ions. As part of the program, also the complex spectral features have been analyzed and possible effects of post-implantation annealing procedures have been discussed. While this report outlines the current status of the program, further information on any of the specific areas is available from the investigators. The results are also communicated to professional journals.⁴⁻⁶

The report is divided into three major parts; (1) Development of Instrumentation outlined under Experimental Arrangement;

(2) Characterization of GaAs dealing with unimplanted and ion-implanted materials subjected to varying anneal procedures;

(3) Characterization of InP with and without implants and the quaternary alloy InGaAsP. In addition, a section describing a first attempt at the theoretical analysis of the line shapes in electroreflectance spectra is included.

II. EXPERIMENTAL ARRANGEMENT

Since the first series of experiments by Cardona et al.,² the electroreflectance technique has become a very important and sensitive tool for the study of semiconductors. It provides an accurate and a nondestructive means of topographic scan of carrier concentrations, chemical inhomogeneities, and optical transition energies. The experimental arrangement used in all the studies reported here consists of a fully automated and sophisticated system developed in this laboratory as part of the present project. The usual arrangement of the apparatus for electrolyte electroreflectance makes use of an electrolyte bath shown in Fig. 1a. One electrode is the platinum wire G inserted in the electrolyte while the other electrode is provided by soldering an ohmic contact E to the back side of the sample to be studied. Some techniques involve metal plating of the back surface and subsequent soldering of the electrode. The soldered contact and all but the front surface of the sample are insulated from the electrolyte. As part of our systematic development of a rapid and nondestructive scan of the surfaces, a whole series

of experiments were performed to ensure proper ohmic contact and proper insulation. These processes have been found to be rather difficult and time consuming. In addition, one wants to avoid any damage to the back surface of the samples and also be assured of uniform field across the surface of the sample.

The technique developed in this laboratory is both novel and simplifies considerably the sample insertion in the system. It makes use of a "dual cell" arrangement shown in Fig. 1(b). The configuration consists of two physically separate electrolyte baths and two platinum electrodes immersed in them. It greatly simplifies the many steps involved in the preparation and mounting of the samples before any measurements can begin. Homogeneous field across the surface is ensured and the method is completely nondestructive providing a greatly improved signal to noise ratio.

Fig 2 shows the schematic of the completely automated system developed in this laboratory for rapid EER scans. A McPherson programmable monochromator (Model EU-700) is used to focus radiation of the desired wavelength on to the sample S mounted in the electrolytic cell and fixed to a X-Y translational stage activated by stepping motors. The light sources are either Tungsten lamps (Model Schoeffel LH150) or a tunable laser. The photomultiplier (PM) and usual lock-in techniques are used for measurements. The complete automation of the scan and sampling of as many as a thousand points were achieved through the use of a Tektronix computer graphic display system (Model 4051) in conjunction with an IEEE interface and A/D converter. For the measurement of

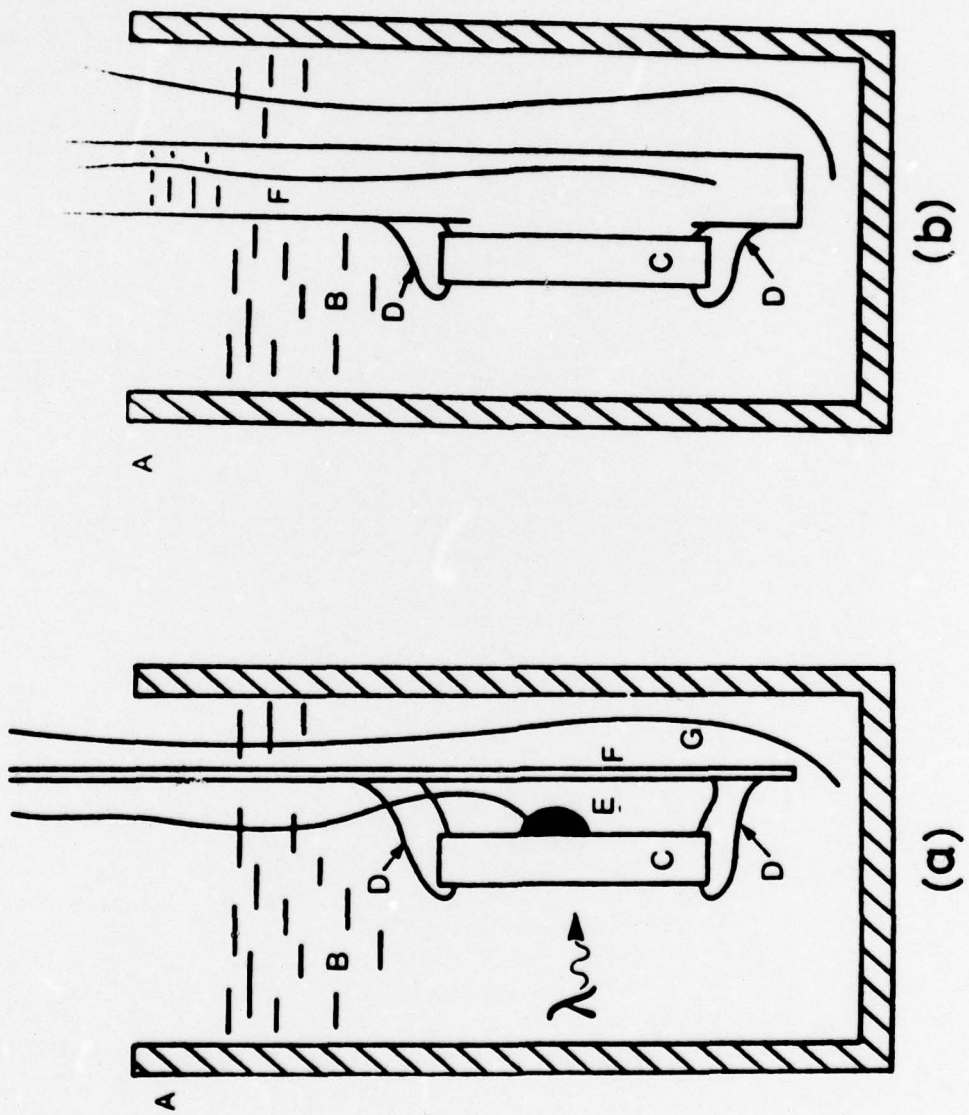


Figure 1

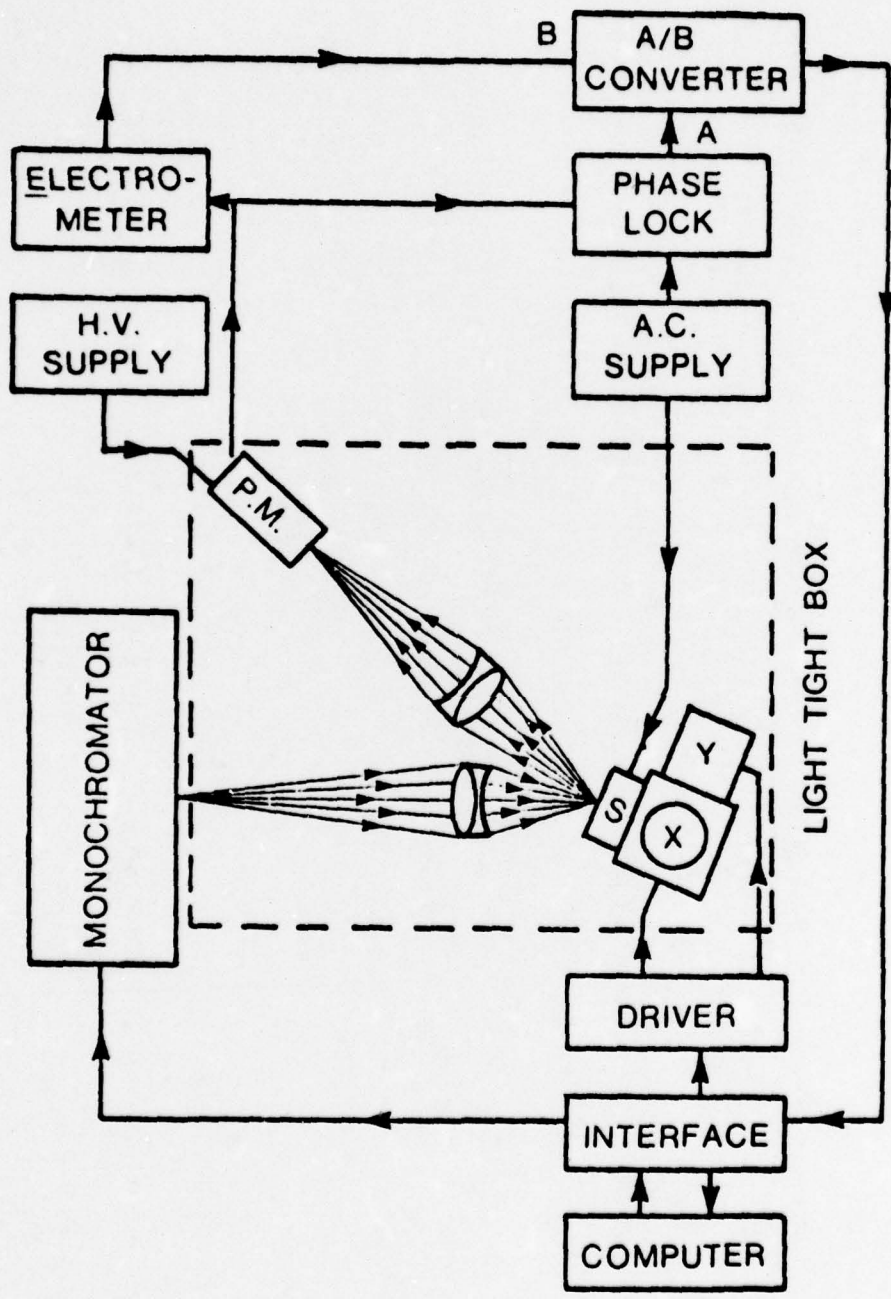


Figure 2

$\Delta R/R$ (change in reflectivity/reflectivity) with modulating voltage, the spot size generally used is $\sim 100\mu$ in the present experiments. However, with tunable laser and appropriate optics attempts are being made to reduce this spot size to $\sim 10\mu$ or less. The spatial resolution is 2.5μ in all our scans.

III CHARACTERIZATION OF GaAs

Introduction

It has been shown that under certain conditions,⁷ the electro-reflectance signal viz, the ratio of the change of reflectivity to the reflectivity is given by

$$\frac{\Delta R}{R} = - \frac{2e}{\epsilon_0} VNL(\lambda, m^*, E_g, \Gamma \dots) \quad (1)$$

where e is the electronic charge and ϵ_0 is the static dielectric constant. V is the modulating voltage applied to the sample, N is the carrier concentration, and $L(\lambda, \dots)$ is the spectral line-shape function which is determined entirely by the band structure. In the case of a uniform material as long as the measurements are taken in the fully depleted space charge layer and the intensity of the light is low enough to prevent appreciable photoexcitation of carriers, Eq. (1) predicts that $\frac{\Delta R}{R}$ is directly proportional to the carrier concentration N . In the configuration used with a dual cell arrangement uniformity of V is ensured. While the condition of uniformity of $L(\lambda \dots)$ is not always met by some of the samples (implanted samples, for example), $L(\lambda, \dots)$ provides us with a convenient means of analyzing the effects of fluence of implanted ions and anneal.

A. Unimplanted Samples of GaAs

The experiments were carried out with three unimplanted samples of GaAs labelled III-16L, 4-32L, and 5-9L. In all the unimplanted samples which we have examined so far, the electro-reflectance spectra of the band gap E_0 and the associated spin-orbit splitting Δ_0 as well as that of the higher interband transition E_1 and its associated spin-orbit splitting are independent of the position (x,y) at which they are measured on the surface of the sample. It is therefore possible to map out the carrier concentration N as a function of (x,y) .

Fig. 3 shows the spectrum $\frac{\Delta R}{R}$ vs E for the sample 5-9L. Figures 4 and 5 give respectively the contour diagram and the three dimensional diagram for the carrier concentration for the area scanned for 5-9L. The peak positions in energy for E_1 , and $E_1 + \Delta_1$ structures are consistent with earlier measurements¹ while those of E_0 and $E_0 + \Delta_0$ structures are shifted to slightly lower energies, possibly due to impurity effects. The contour plot and the three-d plot show peak to peak variations in $N(x,y)$ of the order of 30%. As can be seen, the topography is lacking strong features. The slight rise from one edge is most likely due to the usual variations in doping which generally follow the Czochralsky whirls thereby more or less mapping out the stress fields generated during growth. Figures 6-8 give similar data on sample 4-32L and as illustrated by Fig. 8 it shows strong irregularities as well as a prominent peak near the center of the sample. This sort of variation is, however,

Scan of GaAs 5-9L

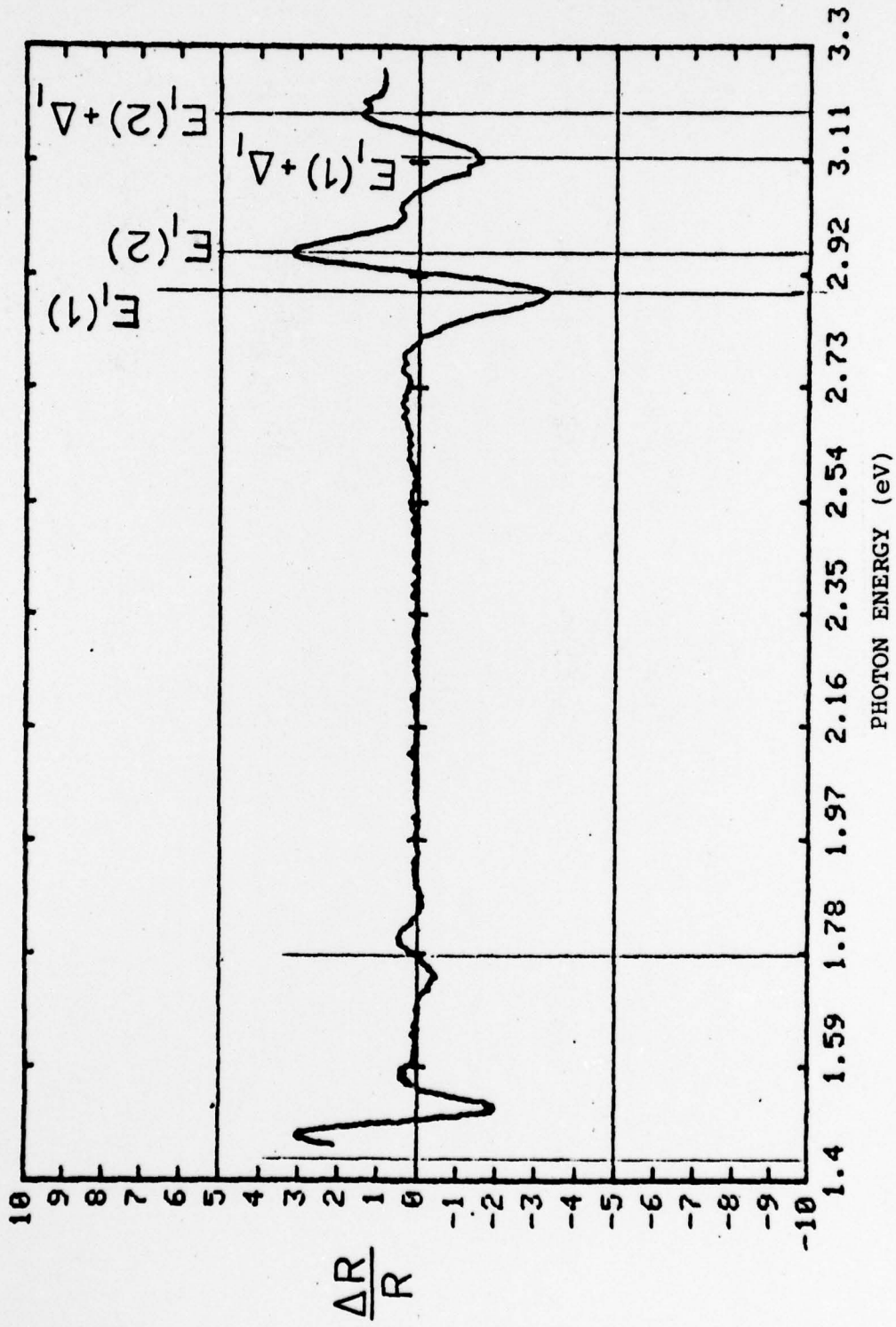


Figure 3

Scan of 5-9L GaAs

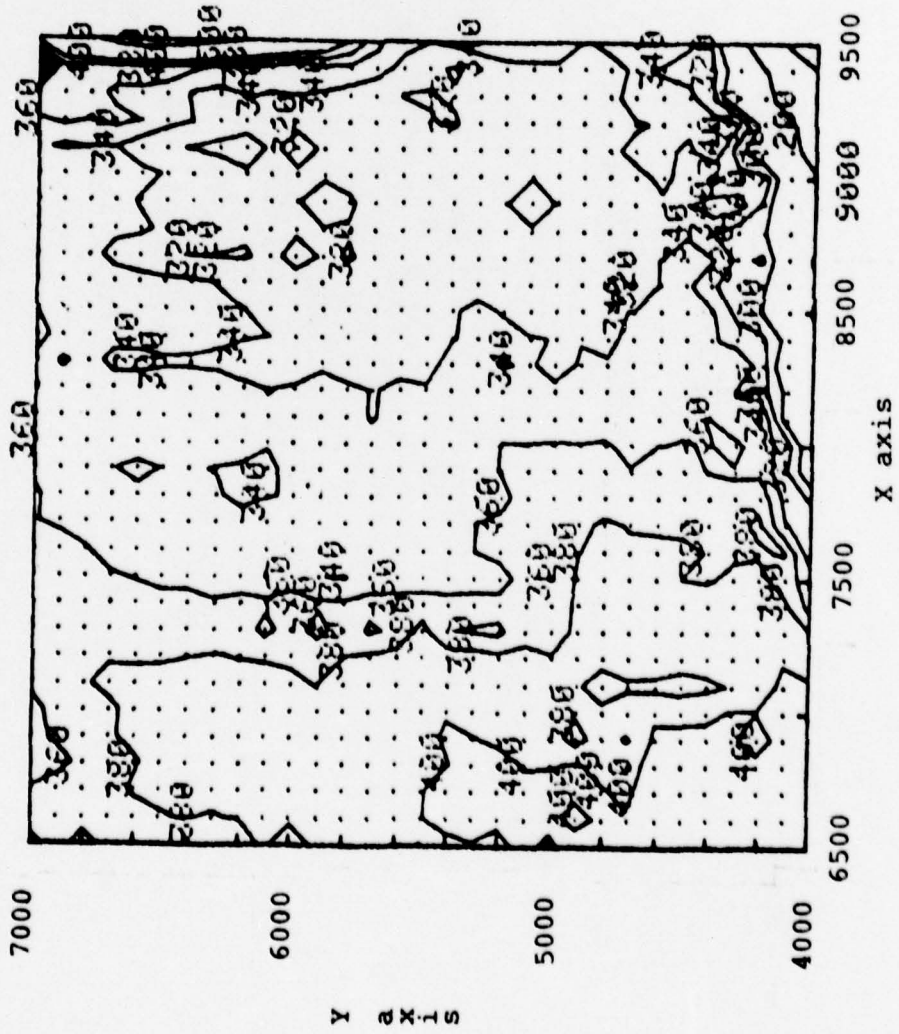


Figure 4

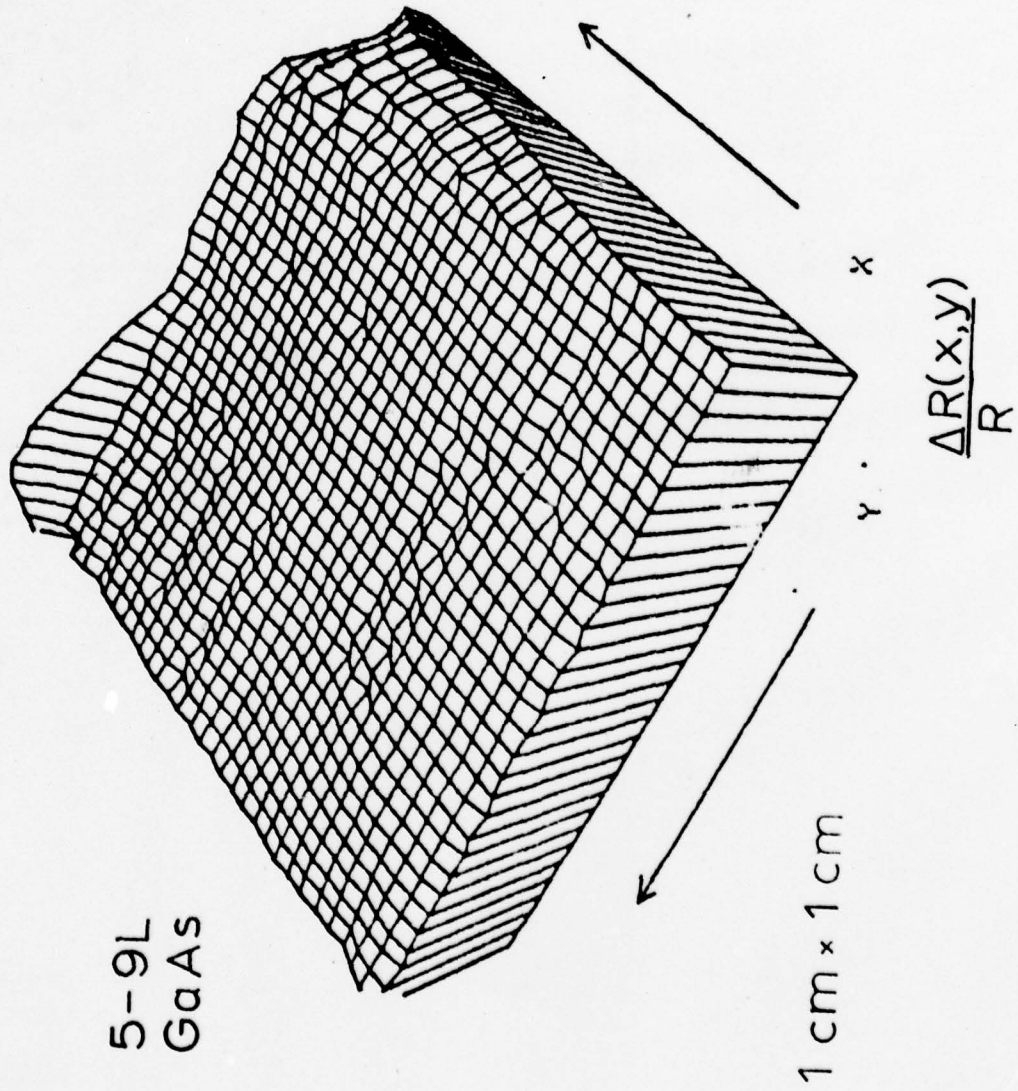


Figure 5

Scan of GaAs 4-32L

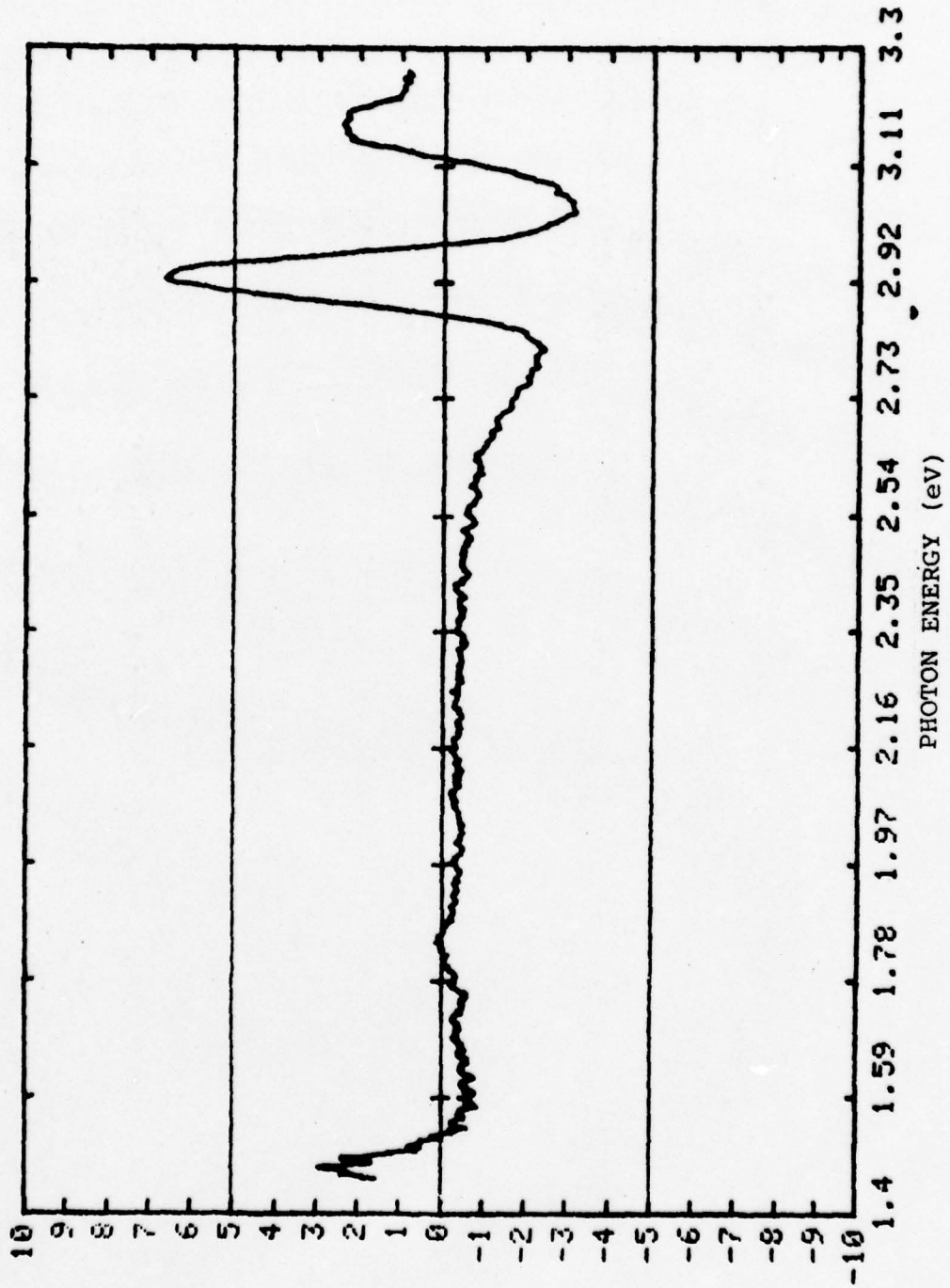


Figure 6

Scan of GaAs 4-32L (P3)

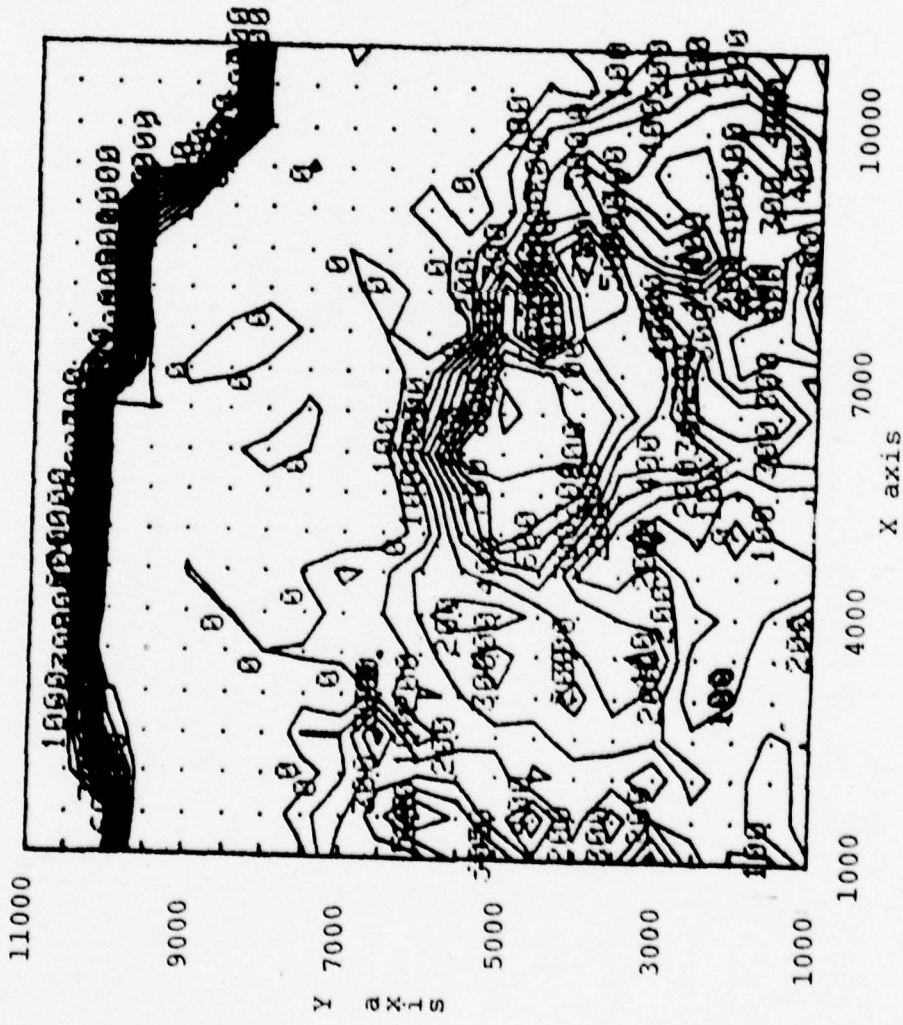


Figure 7

Scan of 4-32L GaAs

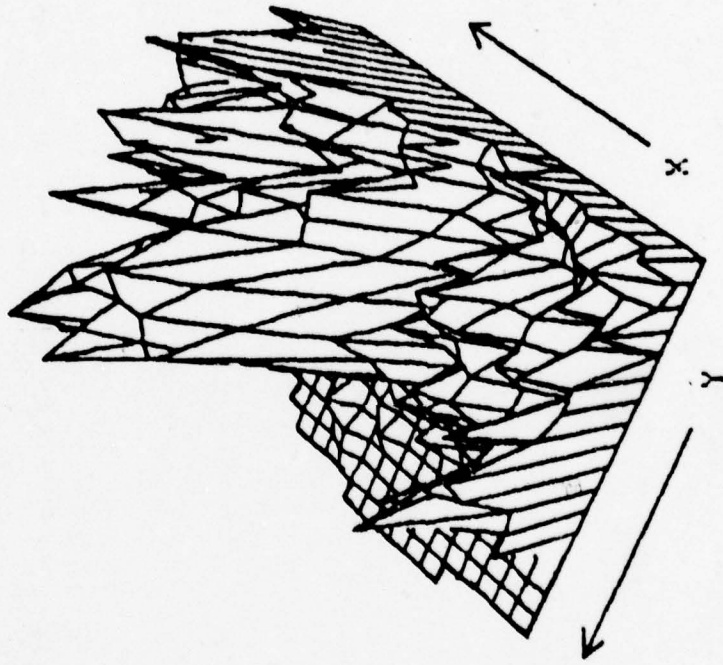


Figure 8

an extreme case for unimplanted samples. E vs $\Delta R/R$ plot for sample III-16L is shown in Fig. 9 and one notices that E_1 structure is altered considerably.

B. Implanted Samples of GaAs

In the next series of experiments, GaAs implanted with Be, Se, Si ions to varying fluences were studied. The first set of implanted samples of GaAs:Be, the fluences are 10^{15} (sample 2185), 2×10^{14} (sample 2186) and 5×10^{13} (sample 2187). Fig. 10 shows a comparison of the E_1 spectra for the unimplanted GaAs (5-9L) and the implanted sample (2185). The unimplanted sample exhibits the well known structure reported in the literature¹ while the implanted sample (Be with 10^{15} cm^{-2} fluence) exhibits a very strong signal and most notably a shift of the structure. The shift of $E_1(2)$ is by 80 meV towards the high energies. In order to study the topographic variation, a particular feature of the spectrum was chosen and in our experiments the zero-crossing (E), close to the transition energy, vs (x,y) was chosen for topographic maps. In Fig. 11 is shown such a variation for the implanted sample 2185 and the topography is lacking strong features, though the energy has shifted by 80 meV. In contrast, as shown in Fig. 12, the topography for sample 2186 (with Be fluence of $2 \times 10^{14} \text{ cm}^{-2}$) is extremely rough. The shift in energy in this case is only +30meV. Clearly in such a case, the topographic irregularities do not result solely from variations in the carrier concentration. When the line shape function $L(\lambda\dots)$ is conserved from place to place on

Scan of GaAs-Cr doped
III-16L

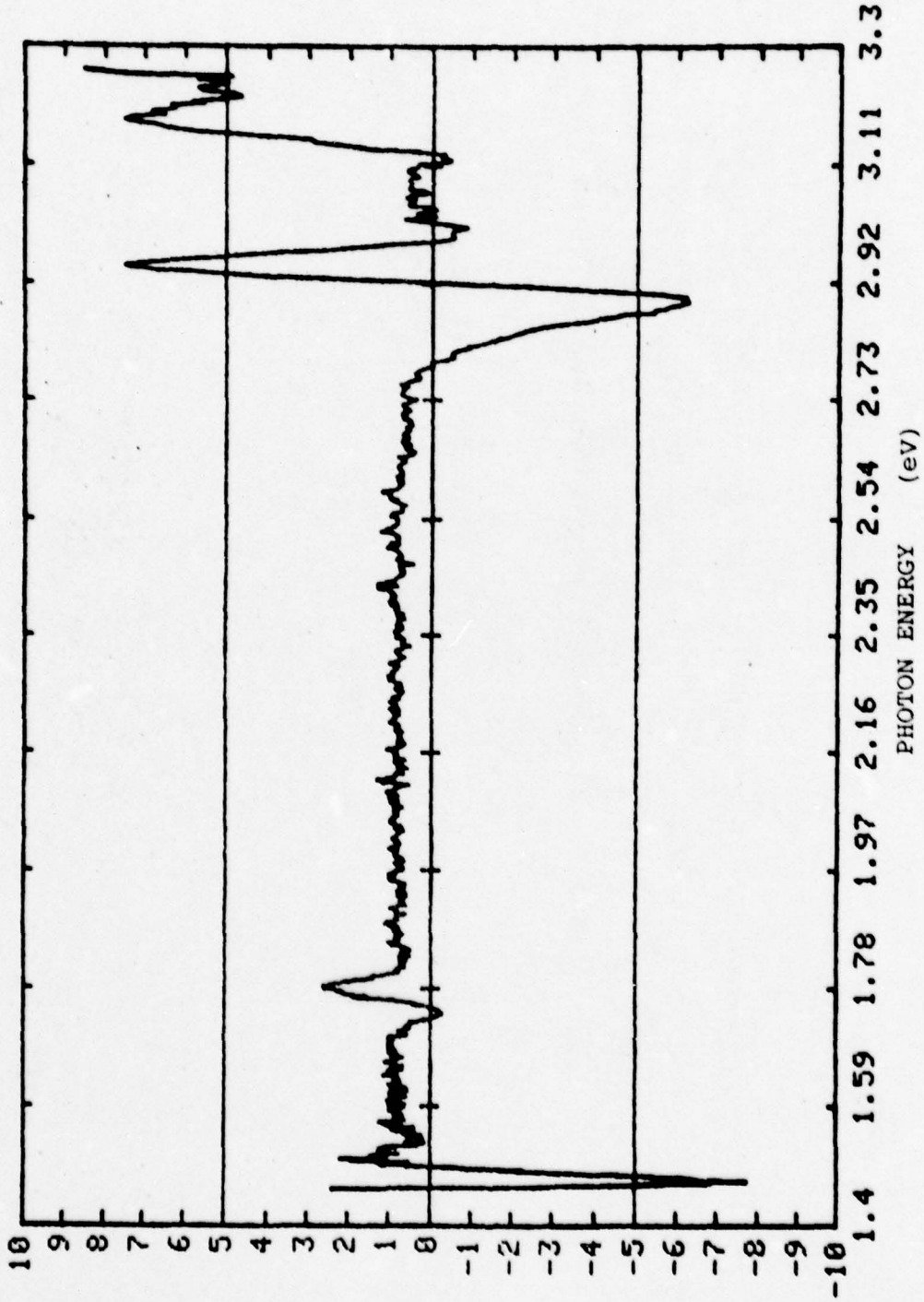


Figure 9

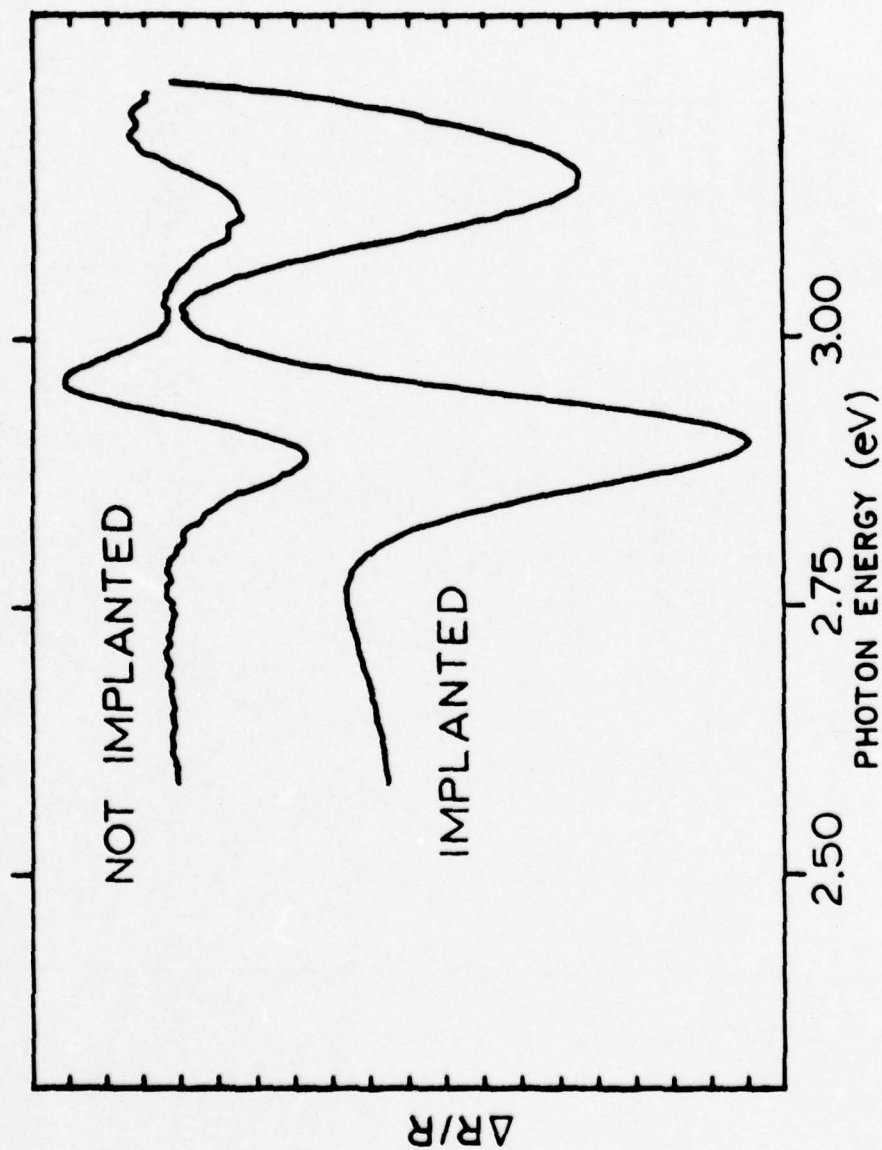


Figure 10

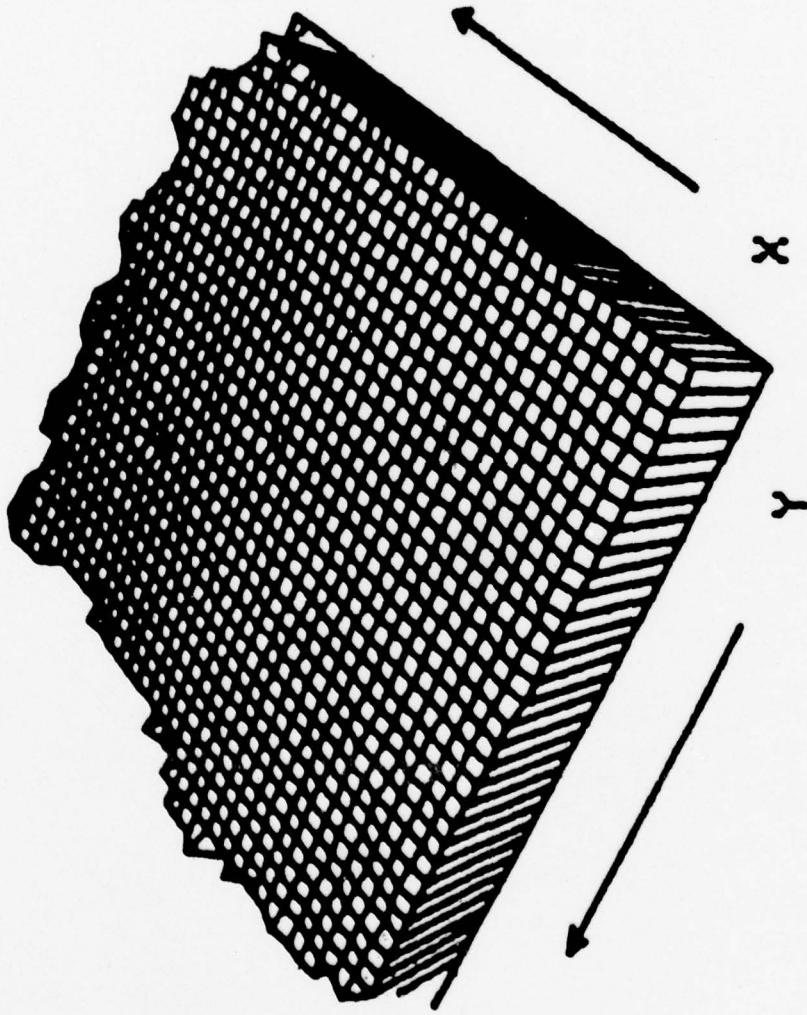
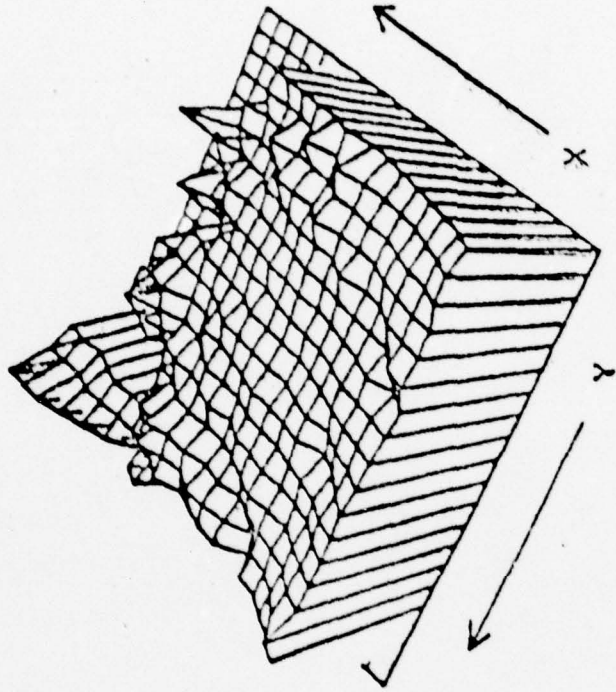


Figure 11



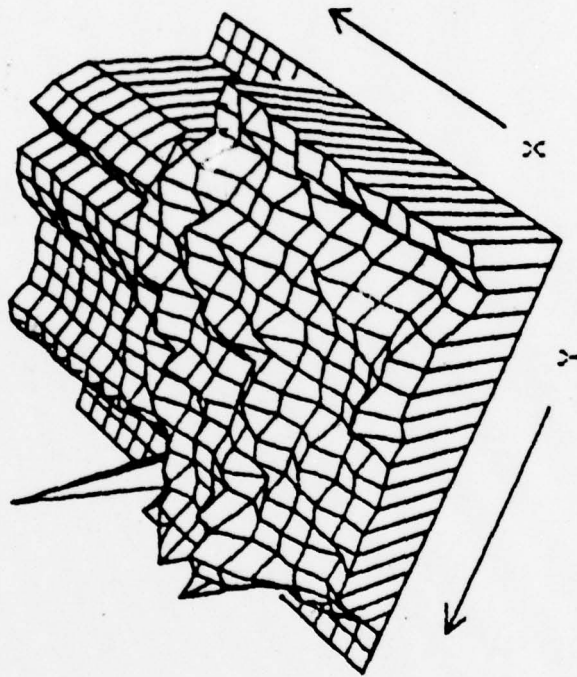
GaAs, Be implant
 $2 \times 10^{14} \text{ cm}^{-2}$, 250 kev
annealed 900 °C

Figure 12

the sample, the scans of $\frac{\Delta R}{R}$ vs (x,y) are always made at a fixed wavelength corresponding to a peak in the electroreflectance spectrum and fairly reflect variations in carrier concentration. However, in sample 2186, the band structure evidently has an (x,y) dependence thus adding an (x,y) dependence to the line shape function $L(\lambda, \dots)$. This is not to imply, however, that the E_1 critical point energy gap is varying. The width, Γ , in addition to E_g determines the ER peak positions. Furthermore, there are additional efforts still under investigation that may relate to these observations. Fig. 13 is an illustration of what is obtained by mapping $\frac{\Delta R}{R}$ vs (x,y) at a fixed wavelength (4191\AA) for the sample 2186. In Fig. 14 the scan $E(x,y)$ for sample 2187 with the lowest fluence ($5 \times 10^{13} \text{ cm}^{-2}$) is quite striking with valleys and craters. As a general rule, the variations in E (of the line shape zero and of the $E_1(2)$ peak) with (x,y) were found to increase with decrease in implant fluence, while the largest shifts with respect to the spectrum reported in the literature occurred for the larger fluences. For example, sample 2185 (10^{15} cm^{-2} fluence) with its large shift of 80 meV for $E_1(2)$ exhibits almost no (x,y) variation whereas sample 2187 ($5 \times 10^{13} \text{ cm}^{-2}$ fluence) with a maximum shift of only 20 meV for $E_1(2)$ shows considerable (x,y) variation.

These observations raise the question of whether these effects are solely due to unannealed lattice damage (left by the passage of the ions during implantation) as seems commonly believed or whether they are due to other causes. In order to resolve the question, two molecular beam epitaxy (MBE) grown samples of GaAs:Be were

Scan of GaAs-Be implant
2186 B



$$\frac{\Delta R(x,y)}{R}$$

Figure 13

SCAN OF GaAs-Be IMPLANTED RUN 2187 "A" N.R.L.



Figure 14

studied. In both of these samples, large positive shifts of $E_1(2)$ were observed. Fig. 15 is a typical spectrum for one of these samples with a shift of + 60 meV. Since MBE grown samples are fairly free of lattice damage it is clear that the analogous changes observed in the E_1 spectrum of Be implanted GaAs samples cannot be due to lattice damage. It would seem that the shifts are rather due to causes similar to those observed earlier on samples with various doping concentrations. In effect, they result from the modifications of the band structure by the impurities.

Generally, it appears that if the lattice is allowed to be mechanically damaged to any great extent, the electroreflectance signal rapidly becomes unobservable due to reductions in amplitude. This was borne out by the absence of signals from either Ar bombarded or Se or Be implanted samples of GaAs that were unannealed. However, in one case, that of a very low fluence (10^{13} cm^{-2}) Be implanted unannealed GaAs sample, we did obtain a signal and were able to compare to that of an identical annealed sample. These two samples are labeled 9127G and 9127F respectively and their spectra are shown in Fig. 16. Note that the unannealed sample had a response magnitude that is 1/20 of the annealed sample. There are appreciable linshape changes but the energy shifts of the $E_1(2)$ peak are similar (~ 20 meV). The unannealed sample shows a broad spectral line shape. Virgin substrate material from the same crystal from which the above two samples were cut, was also examined and the observed peaks were in agreement in the values reported in the literature.¹ This further confirms that the observed shifts are due to impurity effects rather than to unrecovered mechanical damage.

GaAs (Be) MBE

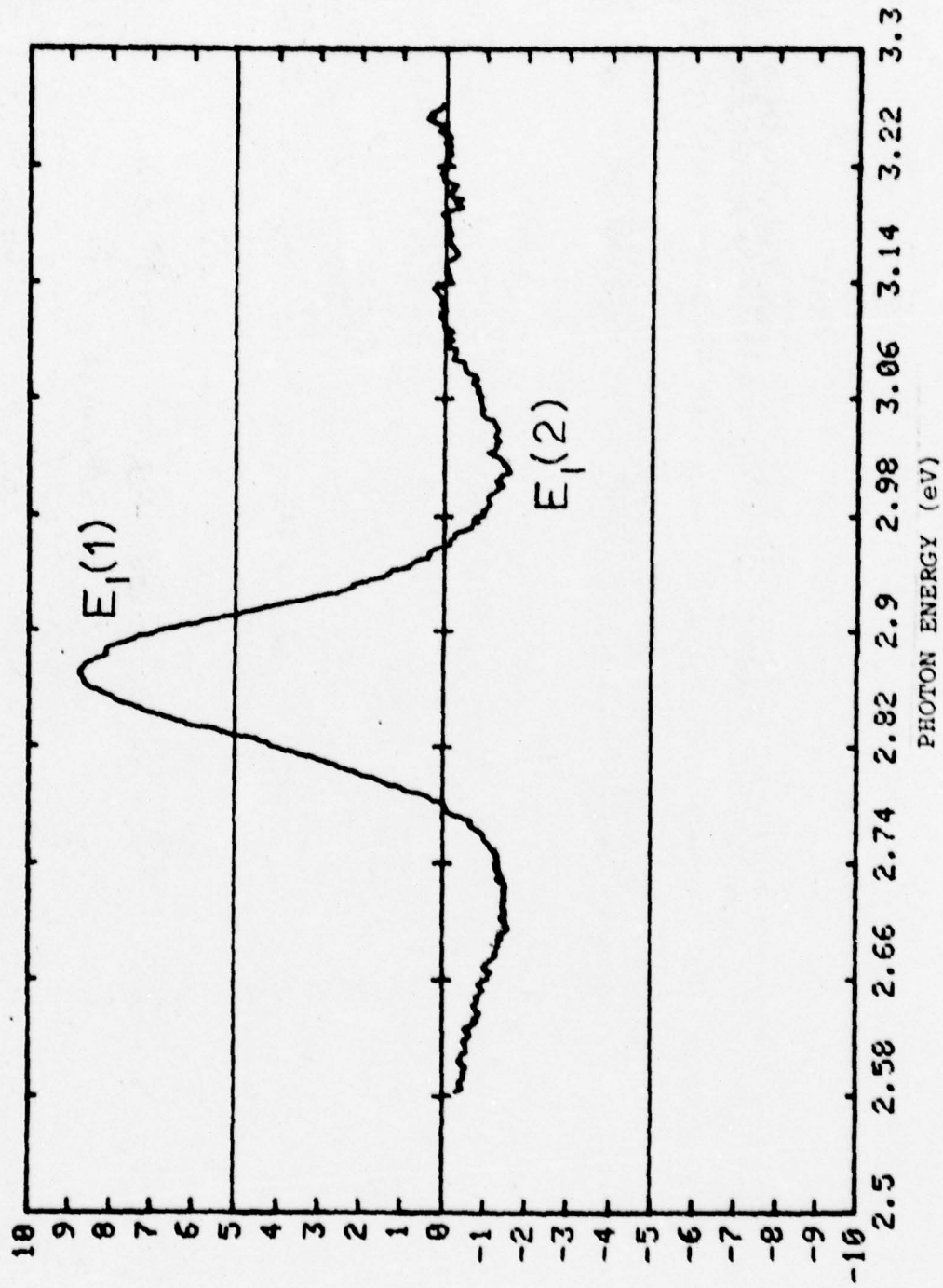


Figure 15

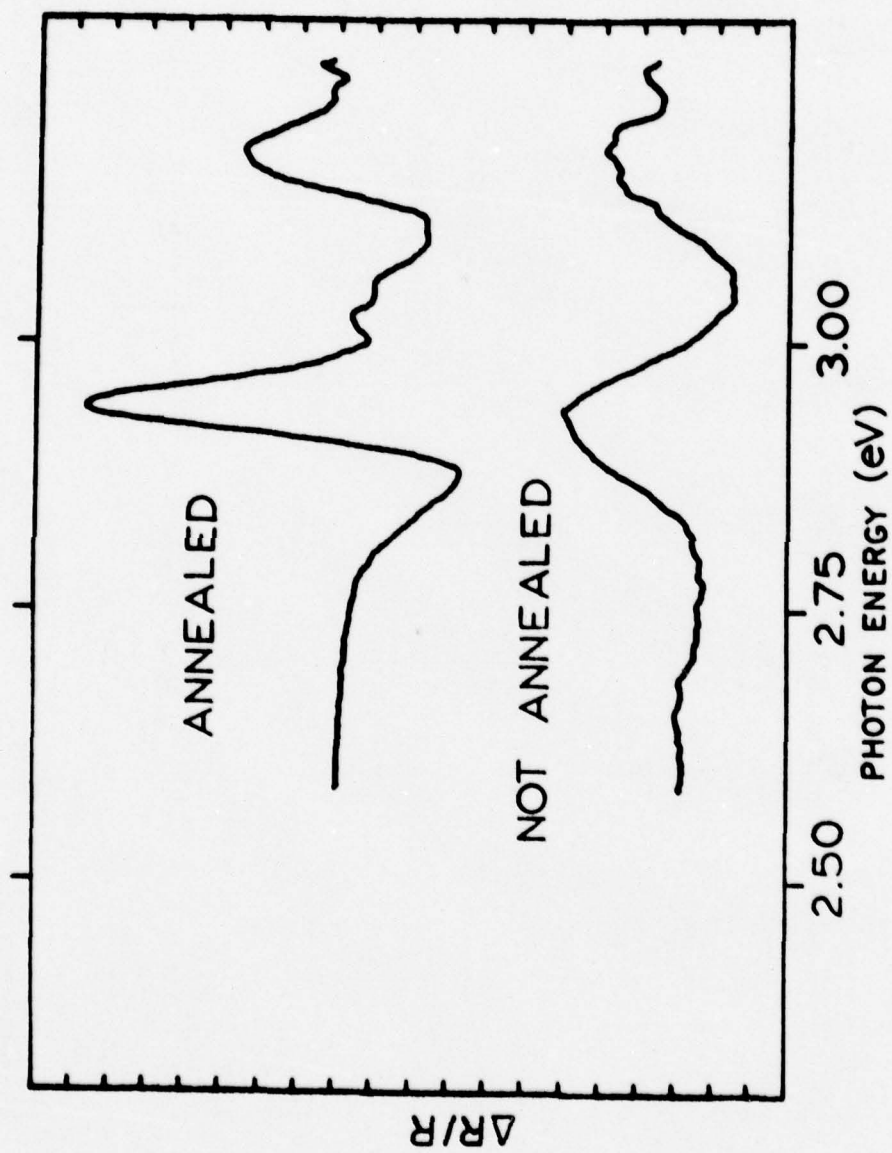


Figure 16

Another interesting result of this investigation is that in certain samples evidence was found that indicates that the inhomogeneity of the implantation had resulted in the formation of p-n junctions in the sample. The power of the electroreflectance technique to characterize the presence of such configurations may be considered the most interesting aspect of the current investigations. This effect was observed in only two of the series of samples in the present studies. The first of these was the unannealed sample with 10^{13} cm^{-2} Be implant. The $\Delta R/R(x,y)$ surface of this sample is shown in Fig. 17. The shape is crater like, with a center where the phase of the $\frac{\Delta R}{R}$ signal is the inverse of the phase of the edges. Fig. 18 illustrates the effect further. Here are shown three traces, taken from points only 0.75 mm apart along the surface of the sample. Since these traces were taken at points of low electroreflectance amplitude, the S/N ratio is small. Nevertheless, the phase inversion noticed as the examined region is moved toward the center of the sample is dramatically clear for the E_1 spectrum. This is not observed in the corresponding annealed sample and so the effect is undoubtedly due to macroscopic clustering of the Be which is normally smoothed out by annealing.

Table I summarizes the data on all the implanted GaAs samples. Figures 19 and 20 present the spectra of GaAs samples implanted with Si and Se respectively. The observed shifts in the $E_1(2)$ peak are all of the same order as in the implanted samples discussed above. In order to prescribe a mechanism to

TABLE I

Sample Identification	Description	Max. Shift of $E_1(2)$
2185	Be→GaAs 250 KeV $1 \times 10^{15} \text{ cm}^{-2}$	+ 80 meV
2186	Be→GaAs 250 KeV $2 \times 10^{14} \text{ cm}^{-2}$	+ 30 meV
2187	Be→GaAs 250 KeV $5 \times 10^{13} \text{ cm}^{-2}$	+ 20 meV
MBEI*	Molecular beam epitaxially	+ 87 meV
MBEII	grown GaAs:Be	+ 60 meV
9127F	Be→GaAs 100 KeV $1 \times 10^{13} \text{ cm}^{-2}$	- 20 meV
9127G	<u>unannealed</u> twin of 9127F	- 20 meV
6-60L Si I	Si→GaAs 170 KeV $5 \times 10^{14} \text{ cm}^{-2}$	+ 46 meV
6-60L Si II	Si→GaAs 170 KeV $5 \times 10^{13} \text{ cm}^{-2}$	+ 64 meV
6-60L Si III	Si GaAs 170 KeV $5 \times 10^{12} \text{ cm}^{-2}$	0 to - 10 meV
LD NCSU	Se→GaAs 300 KeV 10^{15} cm^{-2}	+ 64 meV
BC3S	combination (Be+Se)→GaAs Se at $1 \times 10^{13} \text{ ions/cm}^2$ Be at $5 \times 10^{12} \text{ ions/cm}^2$	+ 10 meV
5 - 9L	unimplanted reference sample of Ga As	No shift

*Provided by Dr. Streetman of the University of Illinois at Urbana

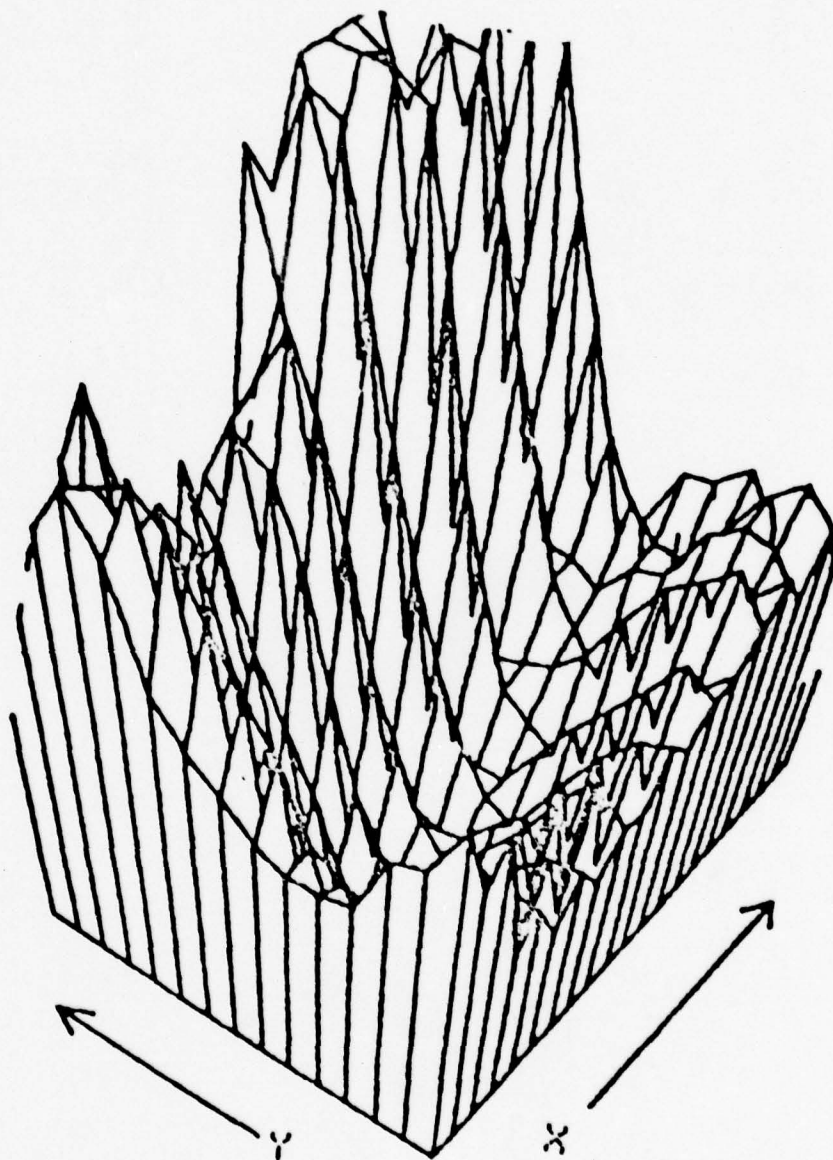


Figure 17

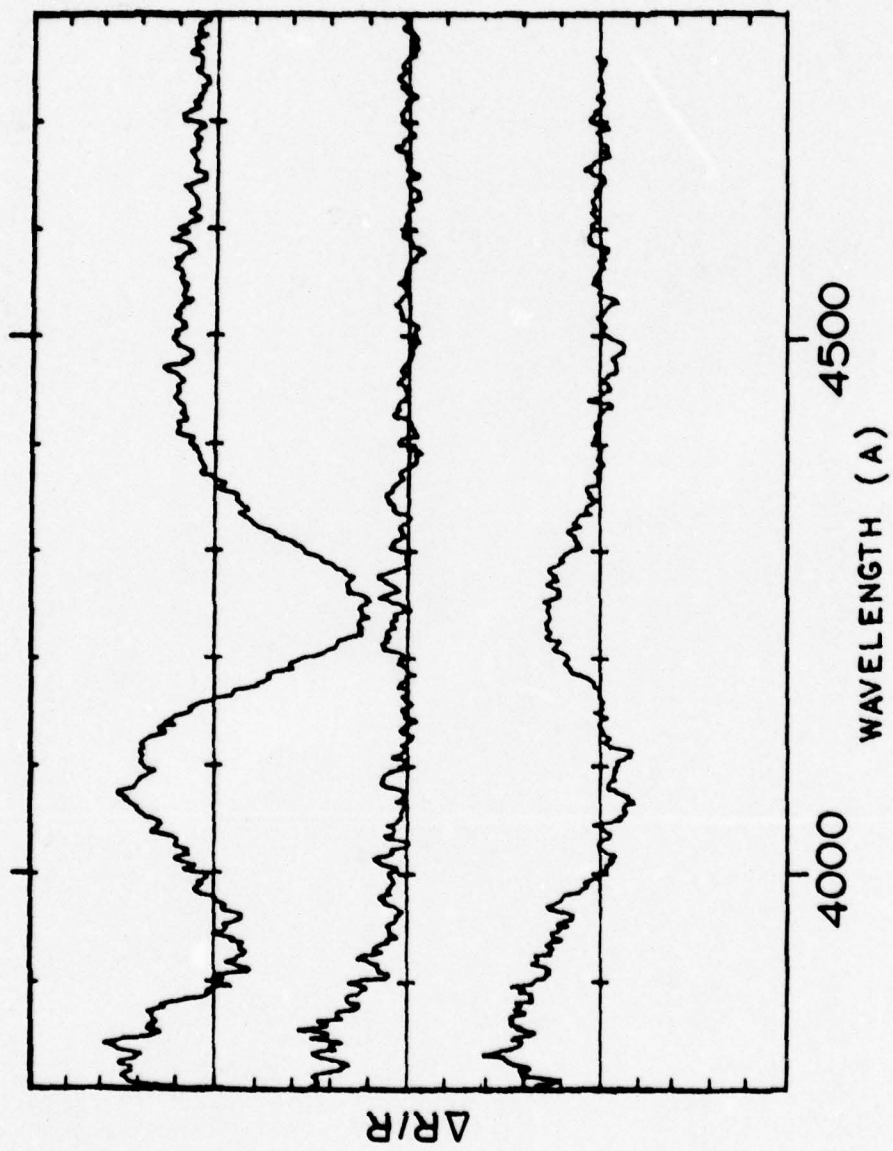


Figure 18

L2 GaAs-Si implant 6-60L
 $5 \times 10^{13} \text{ cm}^{-2}$ (annealed)

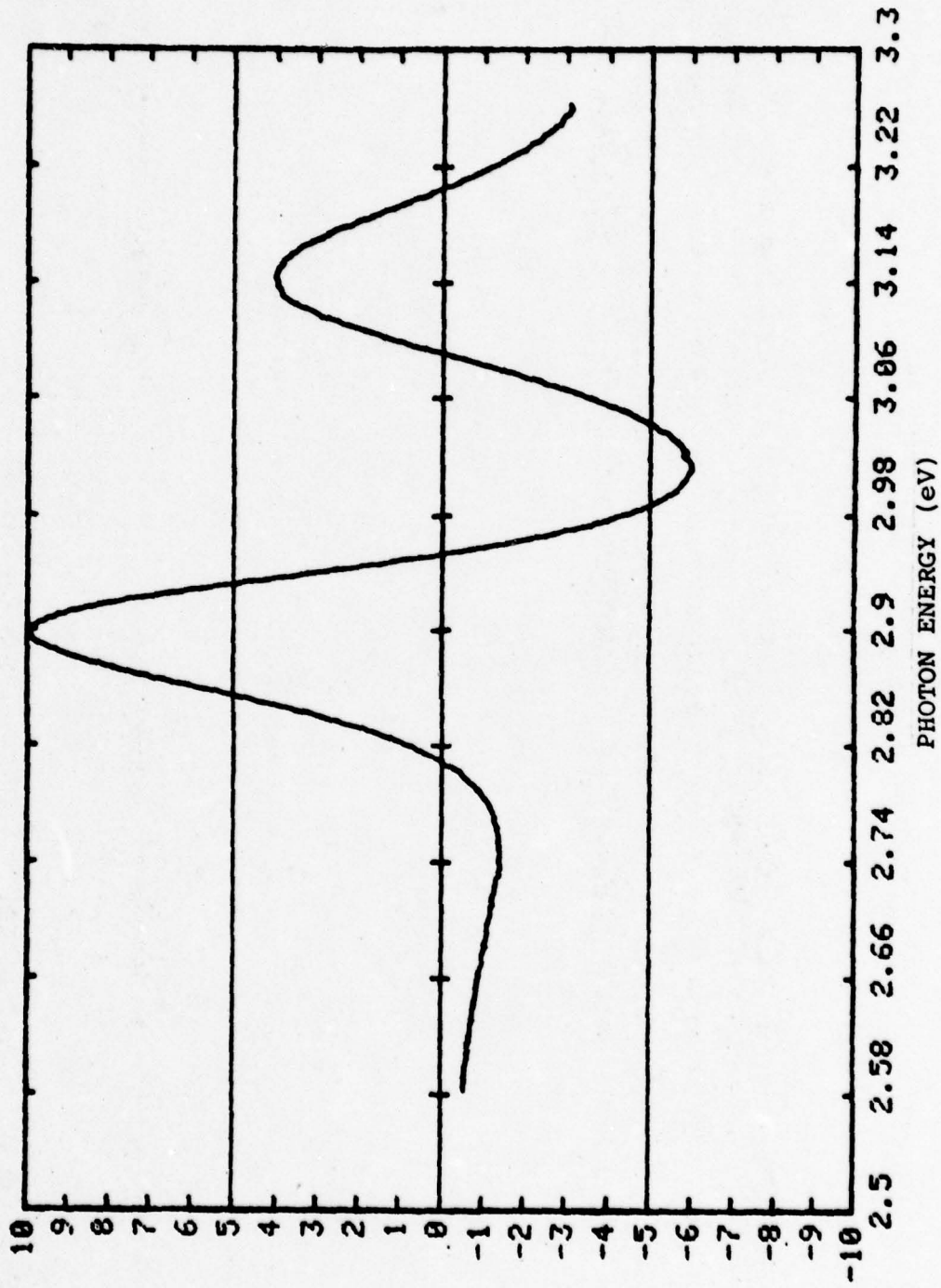


Figure 19

GaAs-Se implant LD NCSU

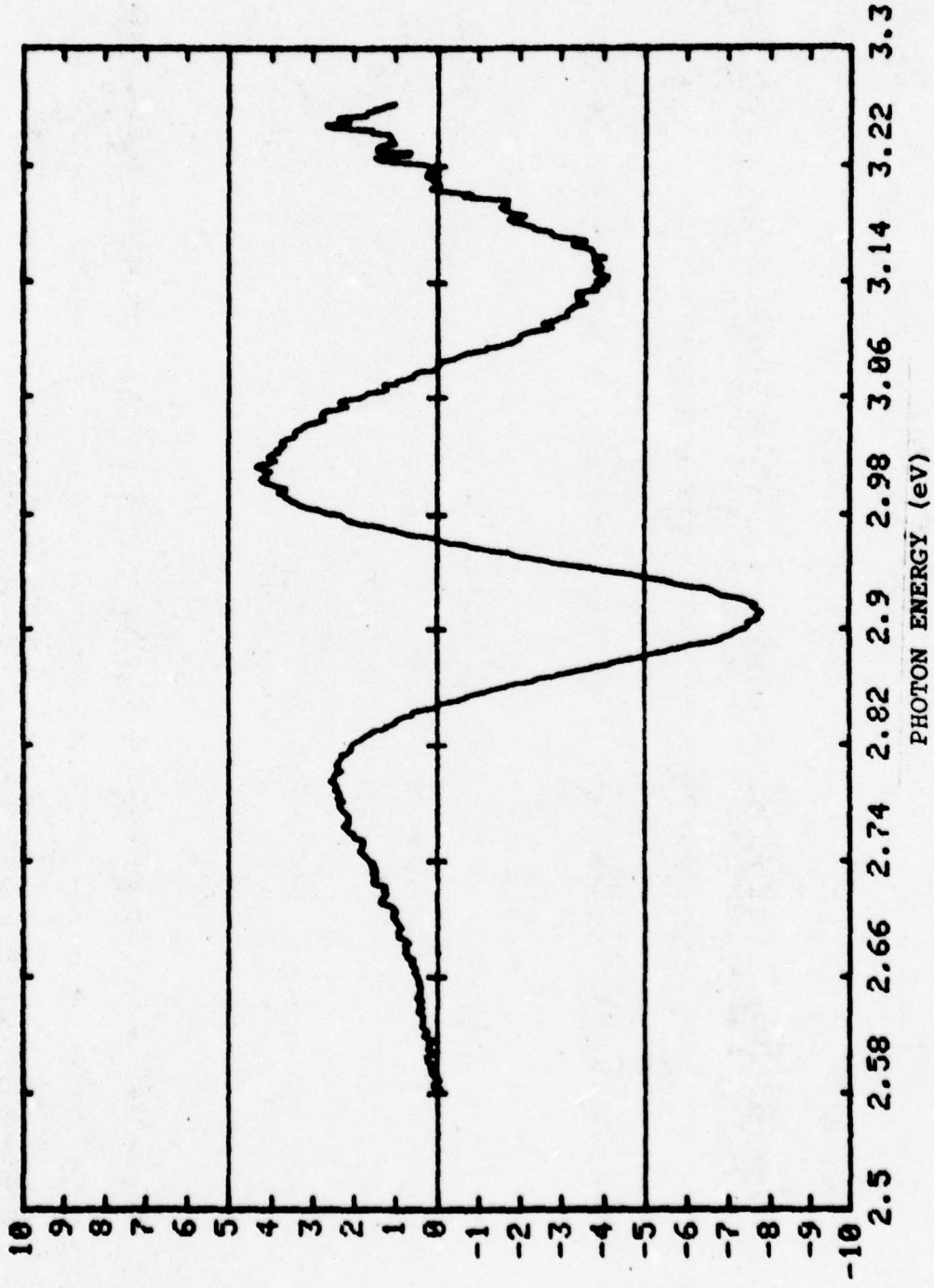


Figure 20

the effects reported here, it is necessary to separate the effects due to E_g and to Γ from the lineshape by a theoretical analysis. Such a program to obtain theoretical "fits" to experimental data is underway.

A similar effect can also be observed as a function of depth of penetration of the incident light. Using the formula for penetration depth,⁸ in the case of GaAs, for example, the incident light corresponding to E_1 transition ($\sim 4260\text{\AA}$) will penetrate $\sim 0.03\mu$ into the sample. The corresponding penetration for wavelengths in the E_0 transition ($\sim 8660\text{\AA}$) will increase to 2.25μ . This range of depths corresponds to the distribution in depth of the Be ions after annealing.⁹ A GaAs sample which was implanted with $5 \times 10^{12} \text{ cm}^{-2}$ of the acceptor Be and $1 \times 10^{13} \text{ cm}^{-2}$ of the donor Se has been investigated. This sample was annealed so that the more mobile Be ions (being less massive than the Se) were distributed closer to the surface. A continuous trace was made of the spectrum covering both the E_1 and E_0 energies. When compared to unimplanted GaAs (as in Fig. 21) it is found that the phase of the E_0 signal is inverted from that of the E_1 . Therefore, the existence of a p-n junction with depth has been inferred.

In summary, we have shown that it is possible to map out the effects of ion implantation with various atomic species in GaAs. The implantation, depending on the fluence, results in modifications both of the free carriers density and of the electronic band states. In relation to the fluence it has been found that the large positive energy shifts resulting from ion implantation

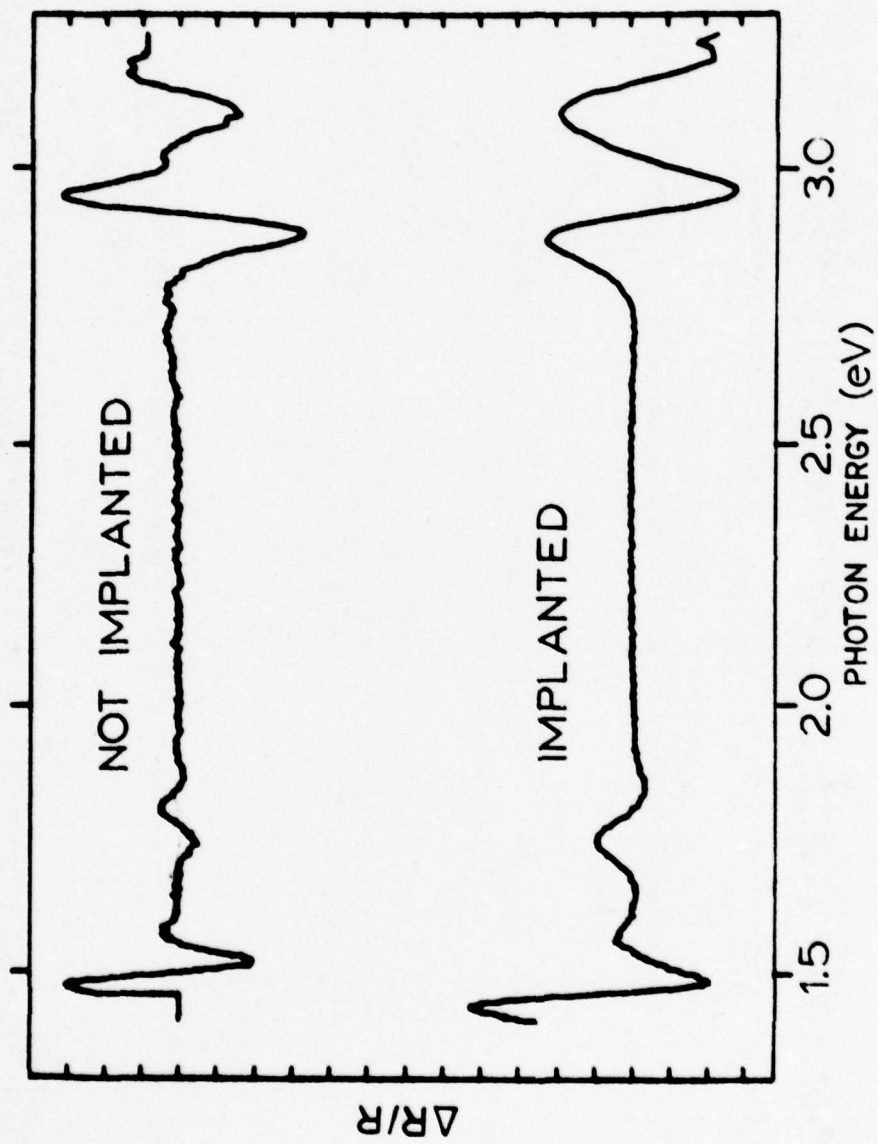


Figure 21

in GaAs result from the ion potential and carrier contributions rather than lattice damage caused by the implantation process and unrecovered by the anneal. Furthermore, the results indicate that it is feasible to spatially structure the optical and electrical properties and generate p-n junctions by controlling the spatial distribution of the implanting ion beam. This has some interesting possibilities for device development.

IV CHARACTERIZATION OF InP

The studies on InP consist of unimplanted samples and samples with Si implant. These samples were all grown at NRL and implanted by the ion-implantation group at NRL. The same electrolyte electroreflectance technique and the automated instrumentation developed in our laboratory were used for investigations of InP, InP:Si, and the quaternary alloy InGaAsP samples.

A. Unimplanted Samples of InP

The first unimplanted sample studied was labeled 1-81-H with Sn doping and Fig. 22 shows the peaks in the E_0 and E_1 regions. The positions of the peaks ~ 1.34 eV and ~ 3.19 eV agree with values reported earlier.¹ In Fig. 23 is shown the spectrum in 3.19 eV region. Very strong signal is obtained and the topographical scan of the surface indicated less than 3% spatial variation of carrier concentration. Using the peak $\sim 3973\text{\AA}$, the carrier concentration plot is illustrated in Fig. 24. Similar results have been obtained for another unimplanted sample of InP (marked as 2-13-H) with Sn and Fe doping. Again $\frac{\Delta R}{R}$ vs (x,y) is very uniform. The spectrum is shown in Fig. 25.

Scan of InP 1-81-H

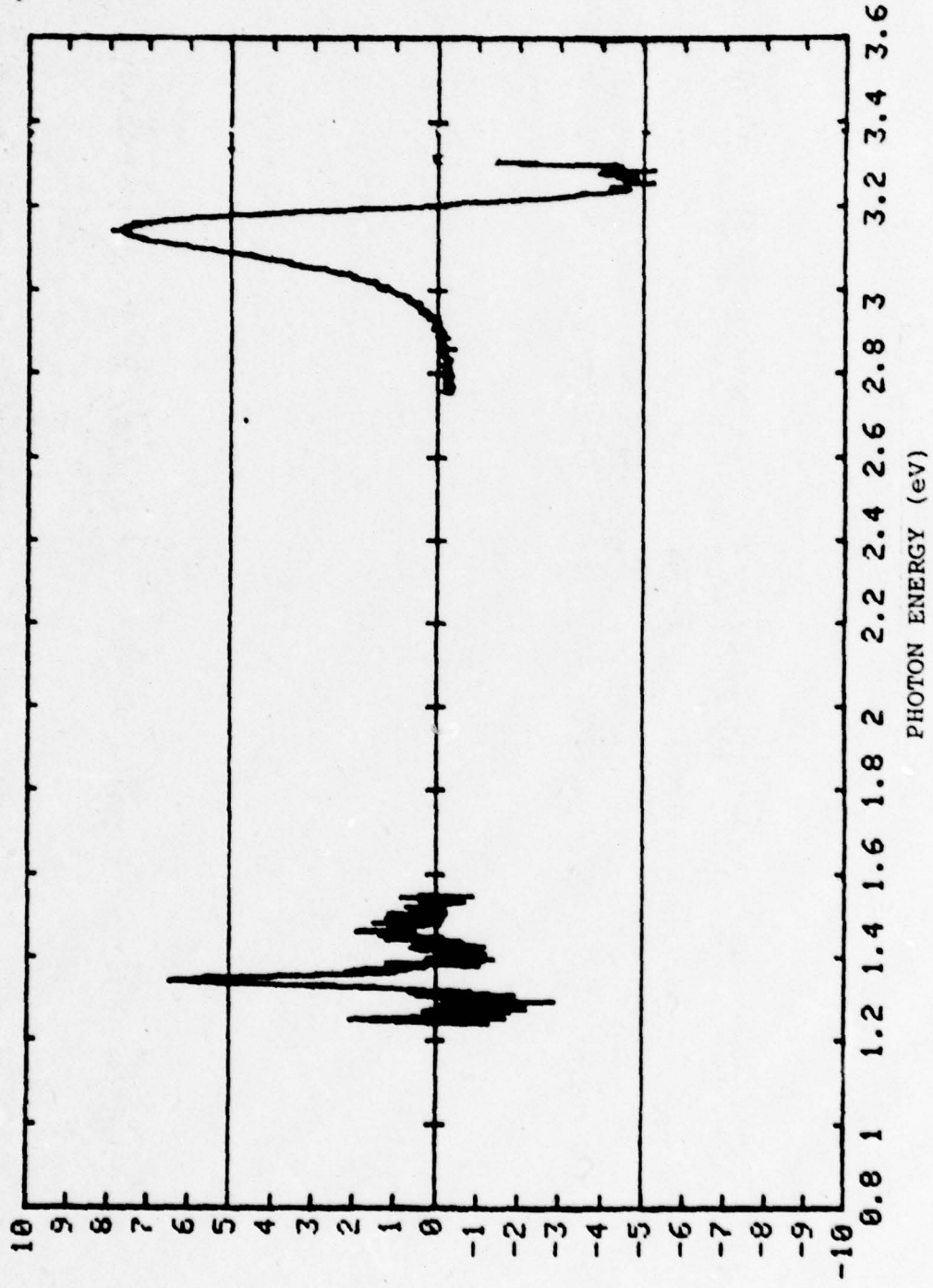


Figure 22

Scan of InP 1-81-H

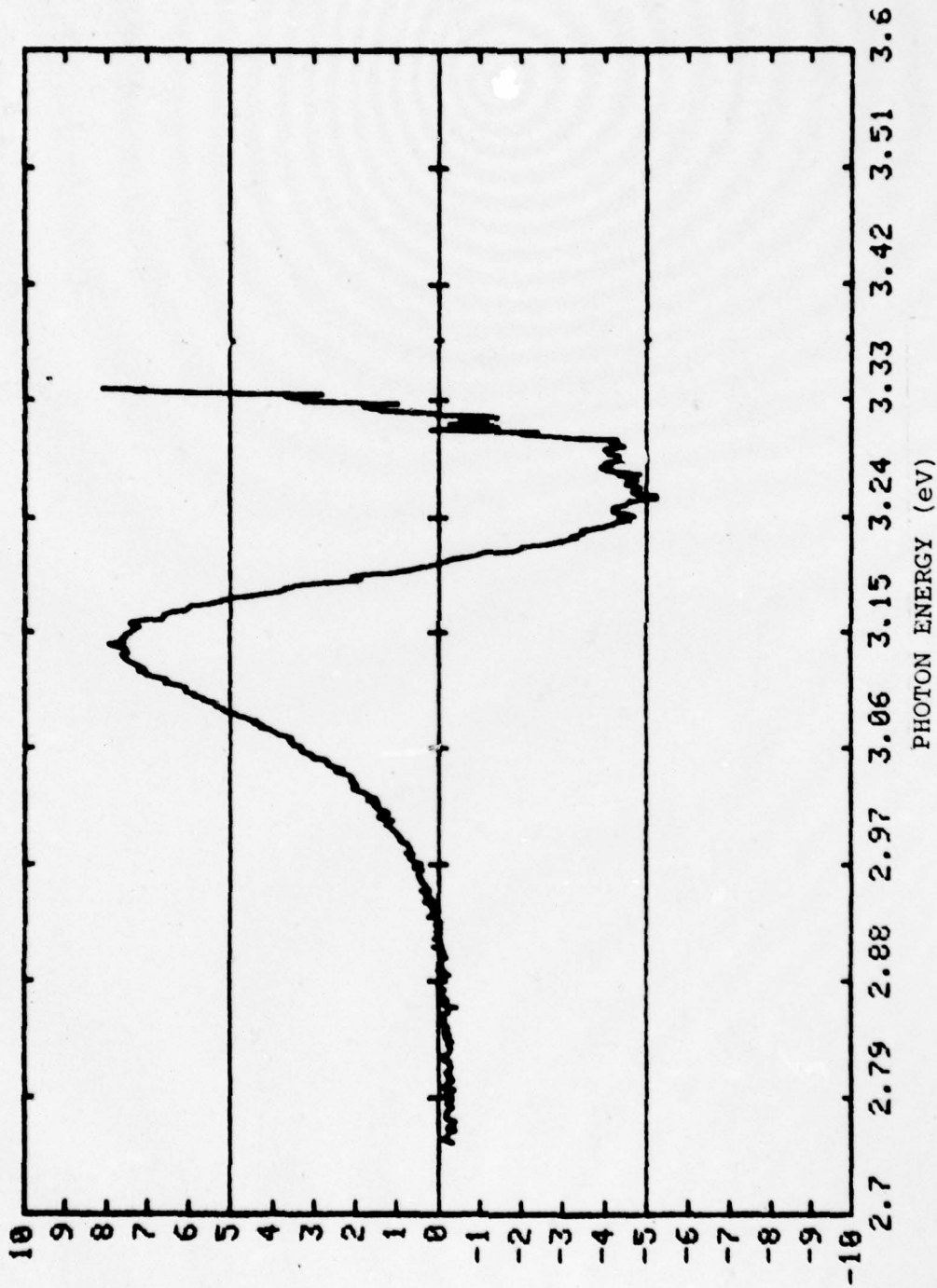


Figure 23

Scan of InP 1-81-H
3973 ang.

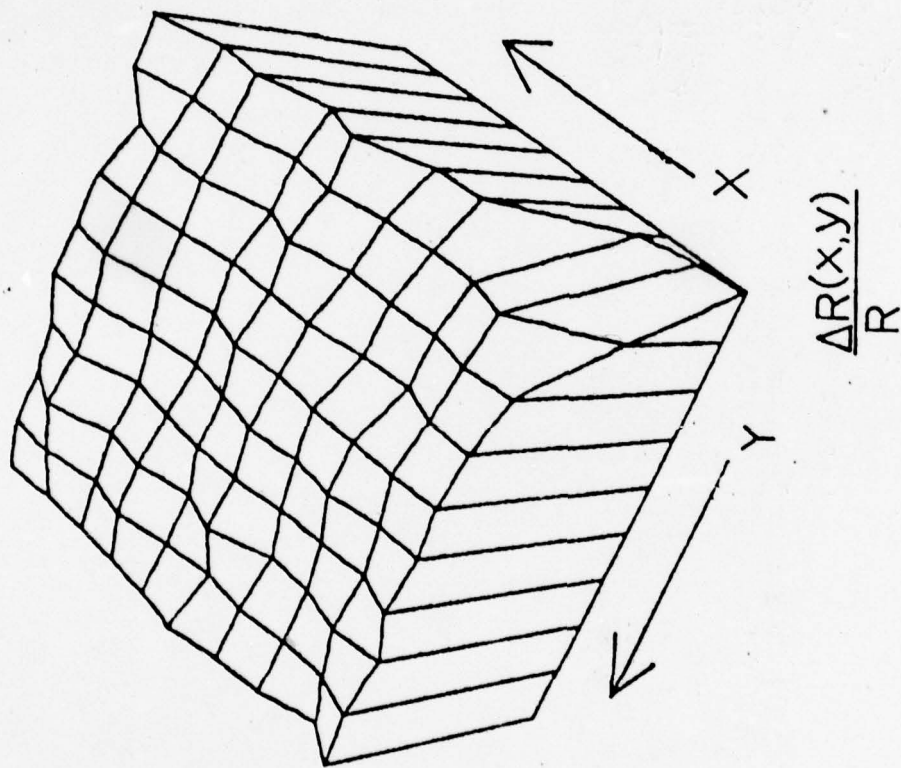


Figure 24

Scan of InP (sn, Fe)
(Sn, Fe doped) 2-13-H

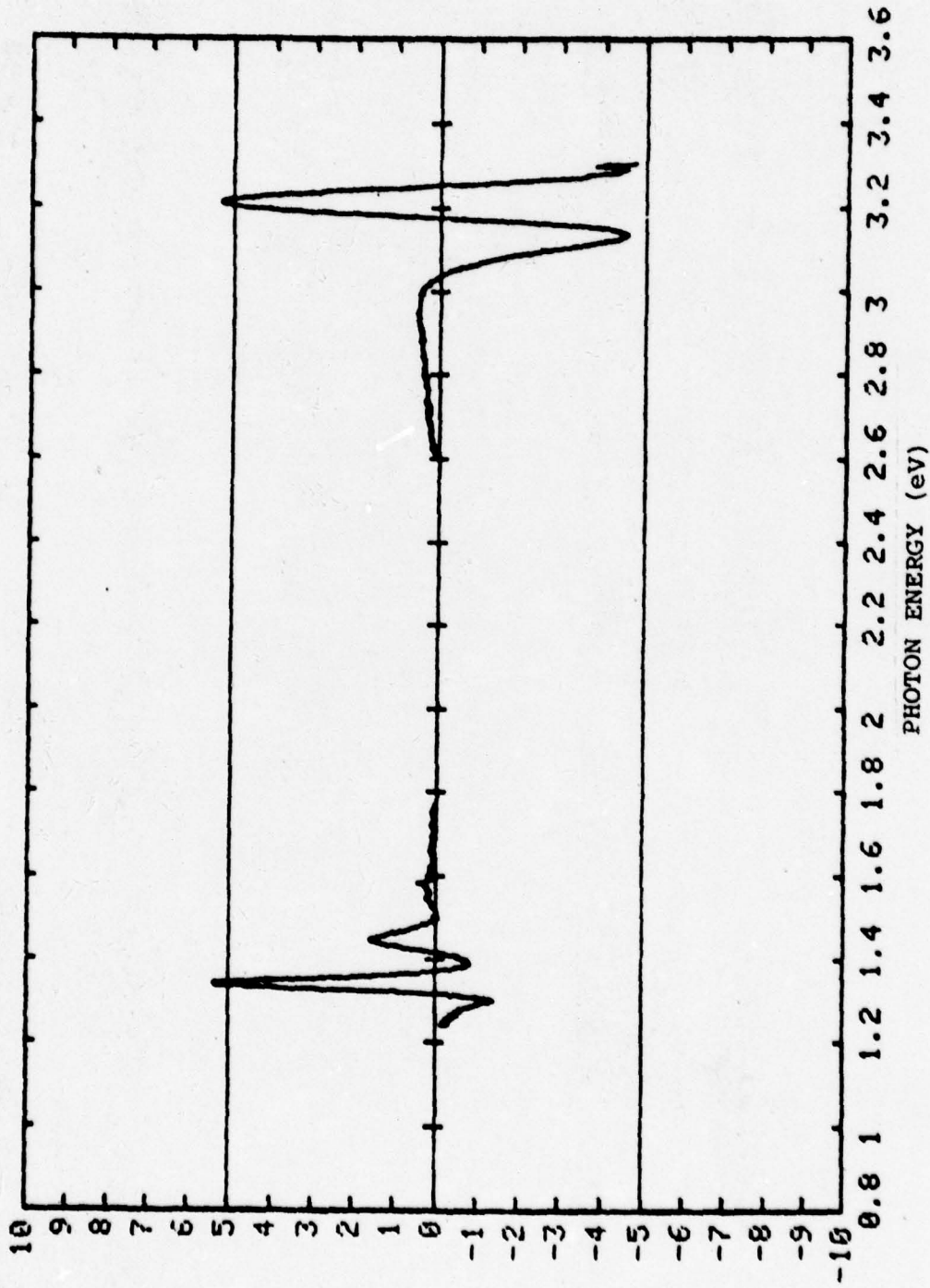


Figure 25

B. Implanted Samples--InP:Si

The studies on samples of InP implanted with Si are in the early stages and as such we have examined only a limited number of samples. The experiments on implanted but unannealed samples did not give a reasonable signal. In the case of implanted and annealed samples, it was possible to obtain enough signal. For the sample with $5 \times 10^{14} \text{ cm}^{-2}$ fluence, the spectrum and the contour diagram for carrier concentration are shown in Figures 26 and 27 respectively. As in the case of GaAs:Si, there is a definite shift of the E_1 peak by $\sim 30 \text{ meV}$. There are spatial variations of carrier concentration as exhibited by Ga As:Si samples. Further experiments in this series of implanted and annealed samples are continuing and the results will be compared with the data on unimplanted samples as well as data on implanted but unannealed samples if reasonably strong electroreflectance signals can be obtained.

C. Quaternary Alloy InGaAsP

As part of our general objective to study the quaternary alloys of III-V semiconducting materials, we have made some preliminary measurements on two samples of InGaAsP (labelled 2-229 and 2-235) kindly provided by Prof. Stillman at Urbana. These samples were grown on InP substrates. The spectral data have been obtained using our EER technique over the significant range of 0.9 eV to 3.6 eV. Both the front and back sides of the two samples have been examined and our results are shown in Figures 28 and 29 respectively for the two samples. In a recent study on this quaternary alloy InGaAsP, Nishino et al.¹⁰ report

Scan of InP-Si implant
L25 (annealed)

$5 \times 10^{14} \text{ cm}^{-2}$

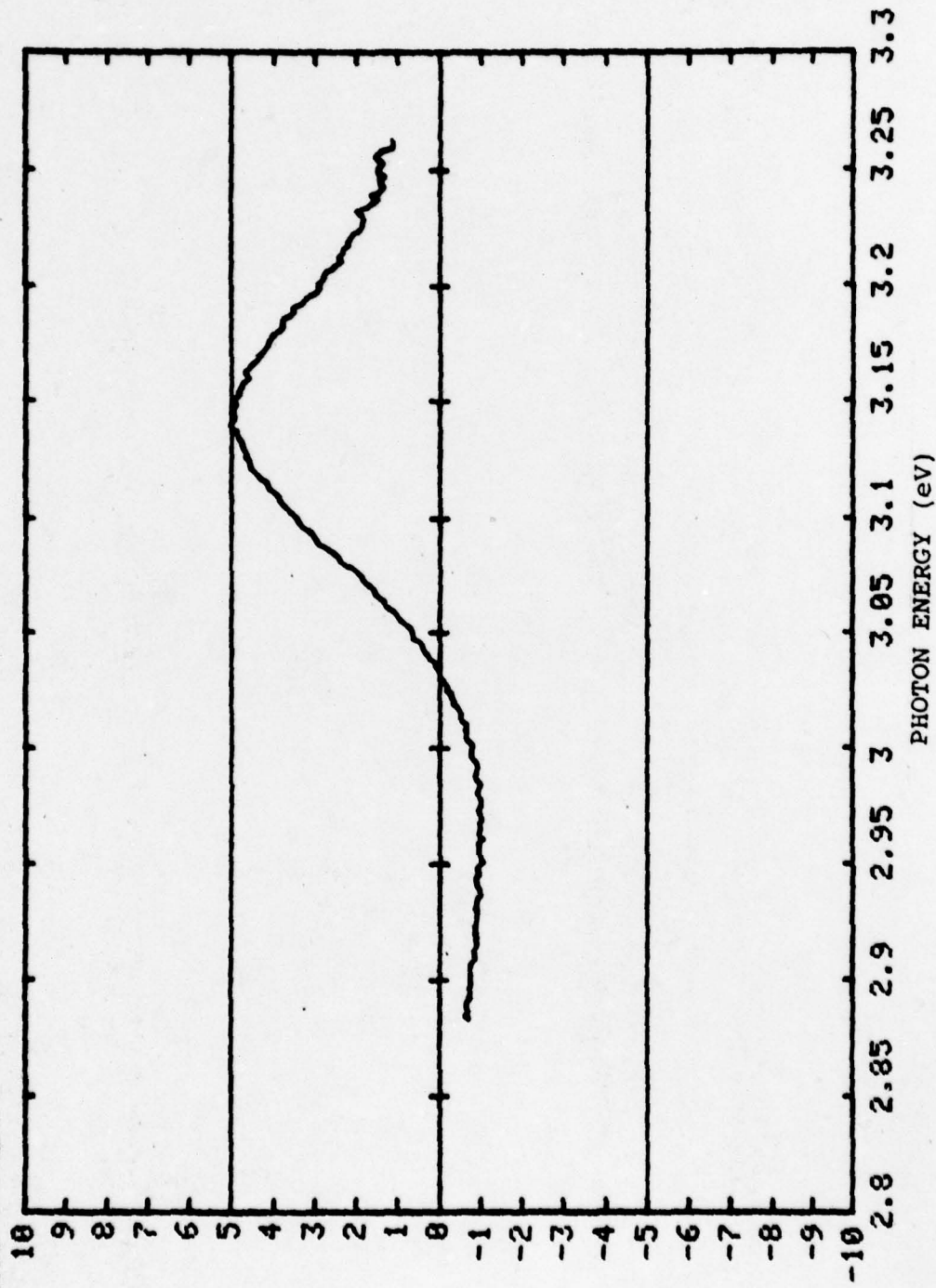


Figure 26

InP-Si implant L25 3950 ang.
 $5 \cdot 10^{14} \text{ cm}^{-2}$ (annealed)

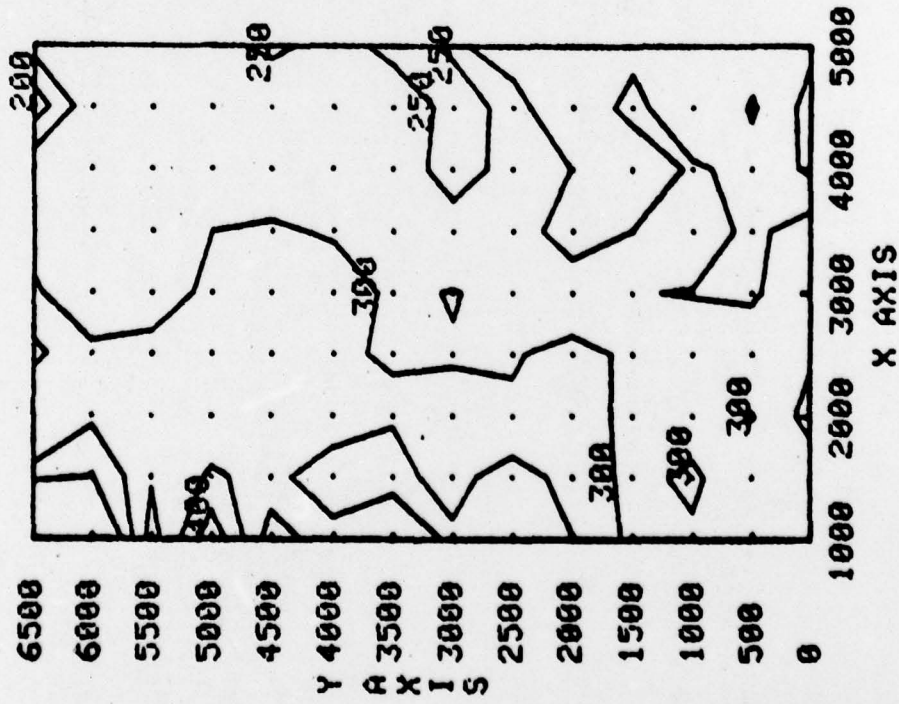


Figure 27

In50AsP 2-229

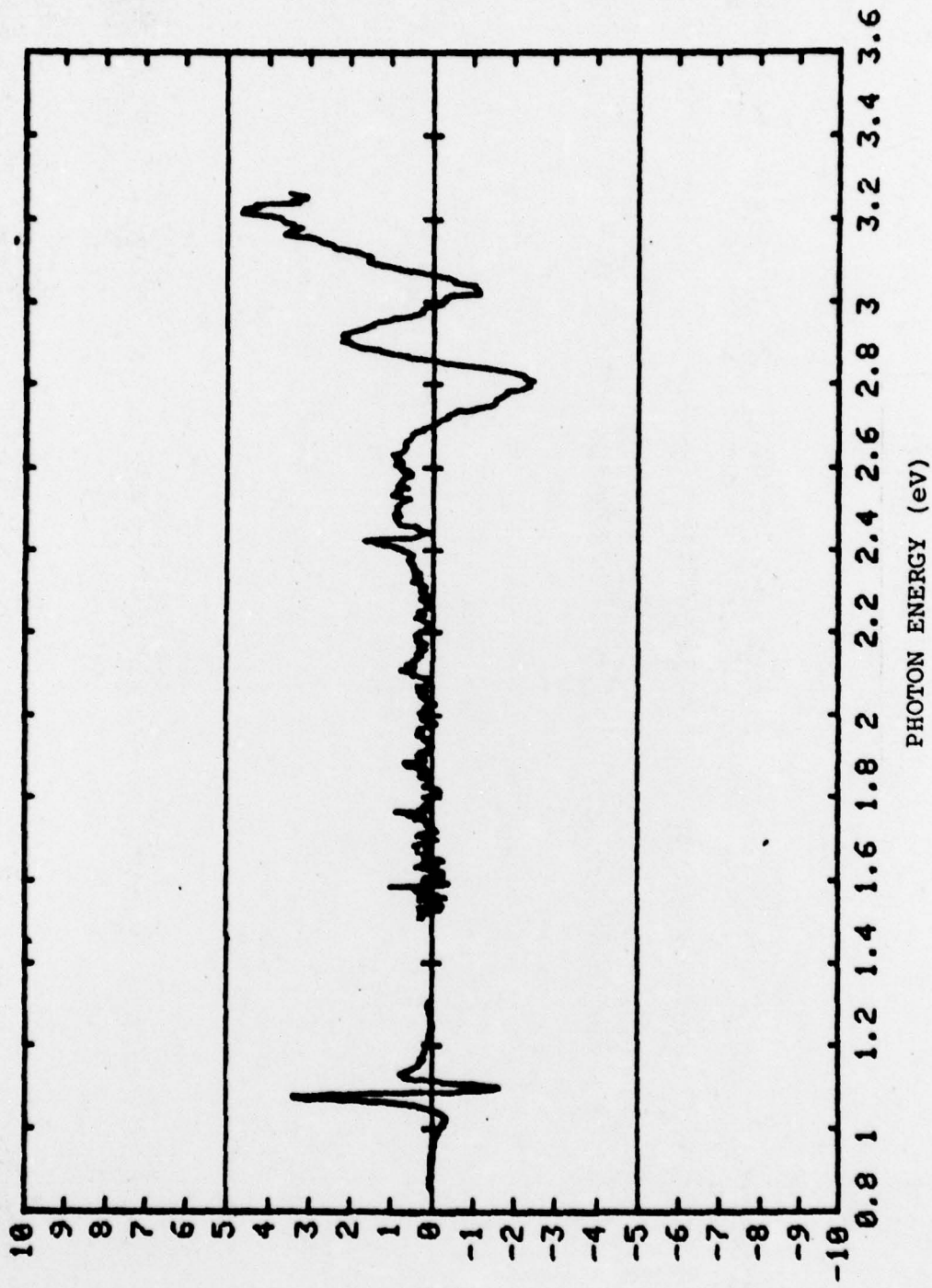


Figure 28

InGaAsP 2-235

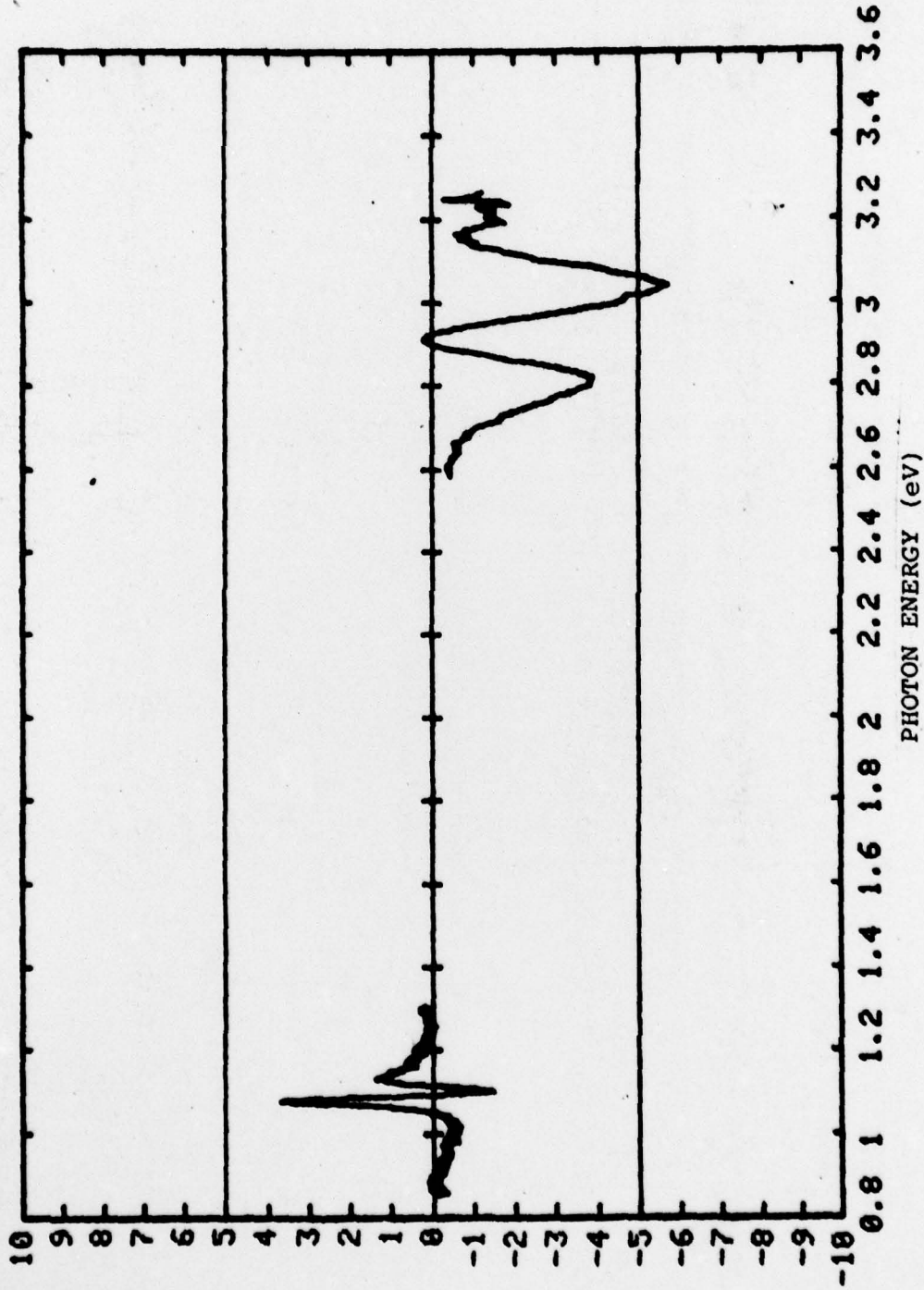


Figure 29

peaks at 1.07 eV, 1.1 eV, 1.17 eV, 1.25 eV, 1.32 eV, and 1.35 eV. Our present results show peaks at 1.075 eV, 1.1 eV, 2.82 eV, 2.92 eV, and 3.05 eV. The peaks at 1.07 eV and 1.1 eV are in excellent agreement with earlier results.¹⁰ However, our experiments did not show any peak near 1.30 eV for the samples we have studied. The substrate side of our samples did show such a peak as one would expect for InP. Also, since the studies of Nishino et al.,¹⁰ do not extend to such a wide range as we covered, no comparison beyond 1.30 eV region is possible. Also, it is important to point out that in such cases where there are several peaks at different energies, it is possible to probe different depths utilizing the different wavelength maxima. As shown earlier in our studies of GaAs, again this is a decided advantage of the powerful electroreflectance technique in the study of different layers of the semiconducting materials.

V ELECTROREFLECTANCE LINESHAPES

It is well known that to obtain sharp highly structured spectra so useful for obtaining the properties of materials, the power of electroreflectance technique is unsurpassed. Admittedly, the determination of the material properties from these spectra is a difficult and uncertain process. However, low field electroreflectance is a convenient and extremely powerful spectroscopic technique for the study of energy band structure. Lineshape problem is particularly significant from a spectroscopic point of view. Hence, as part of our systematic

characterization of GaAs using EER technique, the lineshape problem is being studied.

In order to explain the features of our electroreflectance measurements on implanted GaAs, following the methods discussed by Aspnes¹¹ a theoretical model has been developed for fitting the EER curves. Among the various factors of the lineshape function, as seen in the theory of Aspnes,¹¹ the critical quantity is the broadening parameter Γ which depends on the model assumed for the critical point. Also, the energy gap itself is calculated as another function of the ratio ρ . Thus, in a study of the lineshapes both E_g and Γ have to be considered and we have made a first attempt at developing a line fitting program for the complex spectral features observed in GaAs. As an example, Fig. 30 shows the experimental spectrum and the theoretical curve developed for unimplanted GaAs (sample 5-9L). A broadening parameter $\Gamma = 0.08$ characterizes this spectrum and the gap energy is 2.925 eV. Considering that this is our first attempt to fit the experimental spectra, the agreement between the theoretical model and experimental results seems quite good. It appears that the small reduction in the experimental position at E (Fig. 30) relative to T (Fig. 30) is due to the influence of $E_1 + \Delta$ peak on E_1 . It is planned to make several refinements to improve the accuracy and such work on the theory of lineshapes is in progress.

SCAN OF GaAs 5-9L N.R.L.
energy gap = 2.925 gamma = 0.08

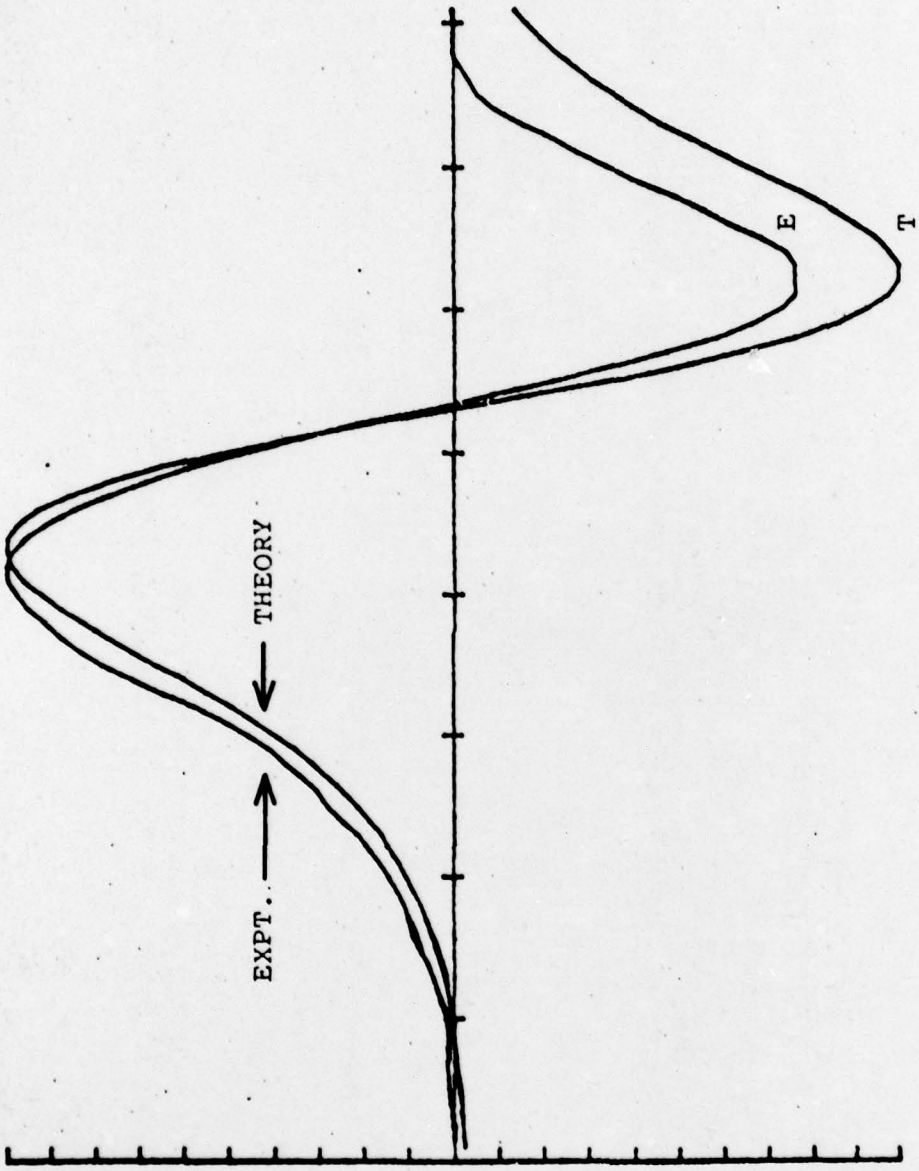


Figure 30

VI ACKNOWLEDGEMENTS

We wish to thank J. Comas and H. Lessoff of the Electronics Technology Division of the U. S. Naval Research Laboratory for providing all the samples and for their suggestions as well as interest in our studies. The support from the Naval Research Laboratory under contract N00173-78-C-0437 is gratefully acknowledged.

REFERENCES

1. M. Cardona, Modulation Spectroscopy (Sections III and VII), Supplement 11, Solid State Physics, Ed. F. Seitz et al., Academic Press, New York, 1969.
2. M. Cardona, K. L. Shaklee, and F. H. Pollak, Phys. Rev. 54, 697 (1967).
3. P. E. Vanier, F. H. Pollak, and P. M. Raccah, Applied Optics 16, 2858 (1977).
4. R. Brown, L. Schoonveld, L. L. Abels, S. Sundaram, and P. M. Raccah, Bull. Am. Phys. Soc. 24, 363 (1979).
5. R. Brown, S. Sundaram, and P. M. Raccah, Bull. Am. Phys. Soc. 24, 365 (1979).
6. R. Brown, L. Schoonveld, L. L. Abels, S. Sundaram, and P. M. Raccah, J. Applied Physics, Submitted 1979.
7. D. E. Aspnes, Phys. Rev. Lett. 28, 93 (1972).
8. Based on formula for penetration depth $d = \frac{\lambda}{2\pi k}$. Values of k are from B. O. Seraphin and H. E. Bennet, in Semiconductors and semimetals, Vol. 3, Ed. R. K. Williamson and A. C. Beer, Academic Press, New York, 1967.
9. H. Lessoff, Private Communication.
10. T. Nishino, Y. Yamazoe, and Y. Hamakawa, Appl. Phys. Lett. 33, 861 (1978).
11. D. E. Aspnes, Surface Science 37, 418 (1973).

Captions for Figures

- Fig. 1. (a) Single electrolytic cell arrangement. A - quartz cell; B - electrolyte; C - sample; D - wax; E - rear ohmic contact; F - supporting palette; G - Pt. electrode immersed in the electrolyte. (b) Dual cell arrangement. Changes are the elimination of the ohmic contact which is replaced by a second electrolyte bath.
- Fig. 2. Block diagram of the electroreflectance system; S - sample, X, Y - positioning motors and PM - photomultiplier. The AC and DC components of the signal are A & B.
- Fig. 3. Spectrum of a GaAs sample with the E_1 spectrum labelled. $\Delta R/R$ is in relative units.
- Fig. 4. $\Delta R/R$ amplitude as a function of the position of the incident light upon the sample surface. The x and y units are in microns. $\Delta R/R$ is in relative units.
- Fig. 5. The three dimensional representation of $\Delta R/R$.
- Fig. 6. Spectrum of a Cr doped sample of GaAs (4-32L).
- Fig. 7. The contour diagram of $\frac{\Delta R}{R}(x,y)$ for the sample 4-32L. X and y are in microns.

- Fig. 8. The three dimensional representation of $\frac{\Delta R}{R}$ for sample 4-32L.
- Fig. 9. Spectrum of a heavily doped GaAs:Cr sample.
- Fig. 10. Comparison of the spectra in the blue (E_1) region of an unimplanted sample (5-9L) and an implanted sample (2185) with a fluence of 10^{15} Be ions/cm².
- Fig. 11. Position in spectral energy of the zero crossing of the E_1 lineshape vs. x-y position, for sample 2185.
- Fig. 12. Display of E_1 (zero crossing) vs (x,y) for sample 2186.
- Fig. 13. $\frac{\Delta R}{R}$ (x,y) for sample 2186 (GaAs:Be with fluence 2×10^{14} ions/cm²).
- Fig. 14. $\frac{\Delta R}{R}$ (x,y) for sample 2187 (GaAs:Be with fluence 5×10^{13} ions/cm²).
- Fig. 15. E_1 spectrum of a molecular beam epitaxy (MBE) sample, GaAs:Be.
- Fig. 16. Comparison of "annealed" and "not annealed" samples (9127) with low Be fluence in GaAs (10^{13} ions/cm²).

- Fig. 17. $\frac{\Delta R}{R}(x,y)$ for GaAs:Be (10^{13} ions/cm²) unannealed sample. The center of the crater-like formation has the opposite sign for the ER spectrum phase compared to the edges of the formation. There is a ring of zero ER signal around the inside wall of this crater.
- Fig. 18. Further illustration of the effect observed in the unannealed 10^{13} ions/cm² fluence GaAs:Be sample shown in previous figure. Here are shown three spectra, differing only in slight positional shifts of the sample with respect to the incident light. These were taken first at 0.75 mm to one side of the zero signal position of Fig. 17, then at the zero position, then at 0.75 mm to the inside of this position. Note the spectrum changes phase (in the $E_1(1)$ and $E_1(2)$ peaks) but the spectral positions are unchanged.
- Fig. 19. Spectrum for a GaAs:Si sample (implanted 5×10^{13} cm⁻²).
- Fig. 20. Spectrum for a GaAs:Se implanted sample.
- Fig. 21. Illustration of the change in spectral phase with penetration depth of the incident light into the sample. The sample was implanted with both Be and Se and then annealed.

- Fig. 22. Spectrum of InP(1-81-H) for the near IR region, a PbS detector was used with a consequent increase in noise.
- Fig. 23. Expanded near UV spectrum of the InP(1-81-H).
- Fig. 24. $\frac{\Delta R}{R}(x,y)$ for InP(1-81-H). X, Y step size was 500 microns.
- Fig. 25. Spectrum of InP(Sn,Fe) (2-13-H). Additional filtering prior to the PbS detector has greatly improved S/N ratio from that of Fig. 22.
- Fig. 26. Spectrum of InP:Si implanted and annealed sample (5×10^{14} ions/cm² fluence).
- Fig. 27. $\frac{\Delta R}{R}(x,y)$ for InP:Si sample.
- Fig. 28. Spectrum of a quaternary sample, InGaAsP(2-229).
- Fig. 29. Spectrum of the quaternary sample, InGaAsP(2-235).
- Fig. 30. Example of a trial fit of a theoretical line shape to actual experimental data. The units of the energy gap (E_g) and of width (gamma, Γ) are in eV.

Distribution List

Mr. Hunter Chilton
RADC/OCTE
Griffiss AFB
NY 13441

Mr. Lothar Wandinger
ECOM/AMSEL/TL/IJ
Fort Monmouth, NJ 07703

Mr. Harry Wieder
Naval Ocean Systems Center
Code 922
271 Catalina Blvd.
San Diego, CA 92152

Mrs. Elizabeth Tarrants
AFML/LTE
Wright-Patterson AFB
OH 45433

Mr. S. A. Roosild
RADC
L. G. Hanscom AFB
Bedford, MA 01731

Dr. John Kennedy
RADC/ETSP
Hanscom AFB
MA 01731

Dr. C. Sahagian
RADC/ETSP
Hanscom AFB
MA 01731

Mr. Don Reynolds
AFAL/DHR
Wright-Patterson AFB
OH 45433

Mr. Max Yoder
Office of Naval Research
Code 427
800 North Quincy St.
Arlington, VA 22217

Dr. L. Cooper
Office of Naval Research
Code 427
800 North Quincy St.
Arlington, VA 22217

Dr. J. Dimmock
Office of Naval Research
Code 427
800 North Quincy St.
Arlington, VA 22217

Dr. Y. S. Parks
AFAL/DHR
Wright-Patterson AFB
OH 45433

Chief of Naval Material
Code 0343
Washington, DC 20360

Dr. George Gamota
Staff Specialist for Research
OUSDRE, Room 3D1079
Pentagon
Washington, DC 20301

Dr. L. Weisberg
OUSDRE
Pentagon
Washington, DC 20301

Dr. R. Reynolds
Advanced Research Project Agency
1400 Wilson Blvd.
Arlington, VA 22209

Dr. L. C. Kravitz
Director of Electronic & Solid
State Sciences (223)
Air Force Office of
Scientific Research, Bldg. 410
Bolling Air Force Base
Washington, DC 20332

Mr. Nathan Butler
Naval Electronic Systems Command
Washington, DC 20360

Dr. L. Sunney
OUSDR&E 3D1079
Pentagon
Washington, DC 20301

Dr. Andy Glista
Naval Air Systems Command
Washington, DC 20361

Mr. J. W. Willis
Naval Air Systems Command
Washington, DC 20361

Dr. A. D. Klein
Naval Air Systems Command
Washington, DC 20361

Dr. H. J. Mueller
Naval Air Systems Command
Washington, DC 20361

Dr. Thomas AuCoin
USAECOM
DRSEL-TL-ESG
Fort Monmouth, NJ 07703

Dr. H. Whitman
U.S. Army Research Office
P.O. Box 12211
Research Triangle Park
Raleigh, NC 27709

Mr. M. Siegmann
NAVMAT, Code 0343
Crystal Plaza 5, Room 1044
Washington, DC 20360

Dr. H. R. Riedl
Naval Surface Weapons Center
Code WR-34
White Oak, Silver Spring, MD 20910

Max Swerdlow (2 copies)
AFOSR/NE, Bldg. 410, Rm. C-213
Bolling Air Force Base
Washington, DC 20332

Defense Documentation Center

Advisory Group on Electron Devices

NRL (standard distribution list) +

Code 5200, 5202, 5203, 5000

5210,

5220 (10 copies)

5230

5250

5260

5270

5280

5290